Clim Dyn
DOI 10.1007/s00382-013-1725-9

On the interpretation of inter-model spread in CMIP5 climate sensitivity estimates

Jessica Vial · Jean-Louis Dufresne · Sandrine Bony

Received: 31 July 2012 / Accepted: 5 March 2013

Abstract This study diagnoses the climate sensitivity, radiative forcing and climate feedback estimates from eleven general circulation models participating in the Fifth Phase of the Coupled Model Intercomparison Project (CMIP5), and analyzes inter-model differences. This is done by taking into account the fact that the climate response to increased carbon dioxide (CO_2) is not necessarily only mediated by surface temperature changes, but can also result from fast land warming and tropospheric adjustments to the CO_2 radiative forcing. By considering tropospheric adjustments to CO_2 as part of the forcing rather than as feedbacks, and by using the radiative kernels approach, we decompose climate sensitivity estimates in terms of feedbacks and adjustments associated with water vapor, temperature lapse rate, surface albedo and clouds. Cloud adjustment to CO_2 is, with one exception, generally positive, and is associated with a reduced strength of the cloud feedback; the multi-model mean cloud feedback is about 33 % weaker. Non-cloud adjustments associated with temperature, water vapor and albedo seem, however, to be better understood as responses to land surface warming. Separating out the tropospheric adjustments does not significantly affect the spread in climate sensitivity estimates, which primarily results from differing climate feedbacks. About 70 % of the spread stems from the cloud feedback, which remains the major source of inter-model spread in climate sensitivity, with a large contribution from the tropics. Differences in tropical cloud feedbacks between low-sensitivity and high-sensitivity models occur over a large range of dynamical regimes, but primarily arise from the regimes associated with a predominance of shallow cumulus and stratocumulus clouds. The combined water vapor plus lapse rate feedback also contributes to the spread of climate sensitivity estimates, with inter-model differences arising primarily from the relative humidity responses throughout the troposphere. Finally, this study points to a substantial role of nonlinearities in the calculation of adjustments and feedbacks for the interpretation of inter-model spread in climate sensitivity estimates. We show that in climate model simulations with large forcing (e.g., $4 \times CO_2$), nonlinearities cannot be assumed minor nor neglected. Having said that, most results presented here are consistent with a number of previous feedback studies, despite the very different nature of the methodologies and all the uncertainties associated with them.

Keywords Climate sensitivity · Feedback · Radiative forcing · Fast adjustment · Radiative kernel · CMIP5 climate model simulations · Climate change · Inter-model spread

1 Introduction

The equilibrium global-mean surface temperature change associated with a doubling of CO_2 concentration in the atmosphere is referred to as climate sensitivity. As it controls many aspects of climate change, including the response of the hydrological cycle and of regional climate features to anthropogenic activities, climate sensitivity remains a centrally important measure of the size, and

J. Vial (✉) · J.-L. Dufresne · S. Bony
Laboratoire de Météorologie Dynamique (LMD), Centre National de la Recherche Scientifique (CNRS), 4 place Jussieu, 75752 Paris Cedex 05, France
e-mail: jessica.vial@lmd.jussieu.fr

J. Vial · J.-L. Dufresne · S. Bony
Université Pierre et Marie Curie (UPMC), 4 place Jussieu, 75752 Paris Cedex 05, France

Published online: 23 March 2013

significance, of the climate response to greenhouse gases (Bony et al. 2013a, b). Unfortunately, climate sensitivity estimates from climate models have long been associated with a large spread (Charney et al. 1979; Randall et al. 2007). This spread, which has not narrowed among the current generation of models (Andrews et al. 2012), remains within the 2–4.5° range.

Attempts to estimate the likely range of climate sensitivity from observations of the current climate or from instrumental or natural archives have not narrowed this range substantially (Knutti and Hegerl 2008). An alternative to this holistic approach consists in constraining observationally the individual processes or feedbacks that control climate sensitivity, especially those which are most responsible for inter-model differences. For this purpose, interpreting the spread of climate sensitivity estimates amongst models constitutes a pre-requisite.

For climate models participating in the Third Phase of the Coupled Model Intercomparison Project (CMIP3), cloud feedbacks were identified as the leading source of spread of climate sensitivity estimates (Bony et al. 2006; Dufresne and Bony 2008; Soden and Held 2006), with a major contribution from low-cloud feedbacks (Bony and Dufresne 2005; Randall et al. 2007; Webb et al. 2006). However, Gregory and Webb (2008) and Andrews and Forster (2008) subsequently pointed out that the atmosphere, humidity and clouds in particular, could exhibit fast adjustments to the CO_2 radiative forcing, and that inter-model differences in cloud adjustments could contribute significantly to the spread of climate sensitivity.

The CO_2 radiative forcing has been commonly taken as the radiative flux change at the top of the atmosphere (TOA) after allowing the stratosphere to adjust to the CO_2 increase (Forster et al. 2007). The reason for using this stratosphere-adjusted forcing rather than the instantaneous CO_2 forcing, is that the stratospheric temperature adjustment occurs on shorter time-scales (i.e., weeks to months) than the long-term climate response (operating over decades to millenia). The same rationale is used now for the tropospheric adjustments to change in CO_2 concentration. As tropospheric adjustments to greenhouse gases are fast and not necessarily mediated by surface temperature changes, they may not be considered as part of feedbacks but rather as part of forcing. Such a distinction matters for models for which the cloud response to increased CO_2 does not depend on surface warming but primarily results from fast tropospheric adjustments. These findings call for a revisit of the concepts of forcing and feedback, of the methodologies used to assess them from model outputs, and of our interpretation of climate sensitivity uncertainties.

The purpose of this study is to interpret the range of equilibrium climate sensitivity estimates from models participating in the Fifth Phase of the Coupled Model Intercomparison Project (CMIP5, Taylor et al. 2012). In Sect. 2, we present the methodologies used to diagnose the radiative forcing and feedbacks of each model by taking into account the tropospheric and land surface adjustments to CO_2. In Sect. 3, these methodologies are applied to CMIP5 model outputs, and model estimates of climate sensitivity are interpreted in terms of radiative adjustments and feedbacks. The inter-model spread of climate sensitivity is quantified, and then decomposed into different contributions related to individual adjustments and feedbacks, and into regional contributions. As the spread of climate sensitivity arises primarily from the tropics, mainly by being the largest region covering half the Earth, we analyze in Sect. 4 inter-model differences in water vapor, lapse-rate and cloud feedbacks. A conclusion is presented in Sect. 5.

2 Data and methodology

2.1 Conceptual framework

Let F and ΔR be a radiative forcing imposed to the climate system and the resulting imbalance in the Earth's radiation budget at the TOA, respectively. The climate system responds to this radiative imbalance by changing its global mean surface temperature ΔT_s, and at any time the climate response opposes the radiative forcing according to:

$$\Delta R = F + \lambda \Delta T_s, \tag{1}$$

where $\lambda(<0)$ is the feedback parameter (Bony et al. 2006; Dufresne and Bony 2008; Gregory et al. 2004). When the climate system reaches a new equilibrium, $\Delta R = 0$ and the equilibrium climate sensitivity ΔT_s^e can be estimated as

$$\Delta T_s^e = \frac{-F}{\lambda} \tag{2}$$

Consider now that the radiative forcing F induces tropospheric adjustments to increased CO_2 concentration ($F_{adj,co2}$), without any change in ΔT_s. The equilibrium climate sensitivity $\Delta T_s^{e'}$ can then also be estimated as:

$$\Delta T_s^{e'} = \frac{-(F + F_{adj,co2})}{\lambda'}, \tag{3}$$

where λ' is the feedback parameter when the adjustments are considered as part of the forcing. If we assume that both equilibrium temperature changes are equals (i.e., $\Delta T_s^e = \Delta T_s^{e'}$), then the relationship between λ and λ' can be written as:

$$\frac{\lambda'}{\lambda} = \frac{F + F_{adj,co2}}{F} \tag{4}$$

Figure 1, which illustrates this reasoning, shows the relationships between the forcings, the feedback parameters

and the equilibrium global mean surface temperature according to the energy balance in Eq. 1, when the adjustments to CO_2 are included in the forcing (in blue) or in the feedbacks (in black). Figure 1 also represents an alternative forcing ($F + F_{adj}$, as defined in Sect. 2.2 and Eq. 12), which we use in this study; this forcing includes tropospheric adjustments to CO_2 while holding the SST fixed, but allowing the land surface to warm.

Under this framework, the imbalance in the Earth's radiation budget at the TOA (ΔR) depends on changes in CO_2 concentration, in surface temperature T_s and in the feedback variables X (where $X \equiv \sum x$ and x—used in Sects. 2.3–2.6—refers to atmospheric temperature, water vapor, surface albedo and clouds). To first order, by neglecting nonlinearities, Eq. 1 can be written in a general form as:

$$\Delta R(\mathrm{CO_2}, T_s, X) \approx \left.\frac{\partial R}{\partial \mathrm{CO_2}}\right|_{T_s,X} \Delta \mathrm{CO_2} + \left.\frac{\partial R}{\partial T_s}\right|_{\mathrm{CO_2,X}} \Delta T_s + \left.\frac{\partial R}{\partial X}\right|_{T_s,\mathrm{CO_2}} \Delta X \tag{5}$$

where on the right hand side of Eq. 5, we now explicitly introduce the stratosphere-adjusted forcing to CO_2 (first term), the Planck response (second term) and the TOA radiative response to changes in feedback variables (third term). Note that there is a logarithmic relationship between the direct CO_2 radiative forcing and the increase in atmospheric CO_2 concentration (Arrhenius 1896): $\Delta R(\mathrm{CO_2}) = \left.\frac{\partial R}{\partial ln(\mathrm{CO_2})}\right|_{T_s,X} \Delta ln(\mathrm{CO_2})$, which does not appear explicitly in the equations of this paper to simplify their writing. There

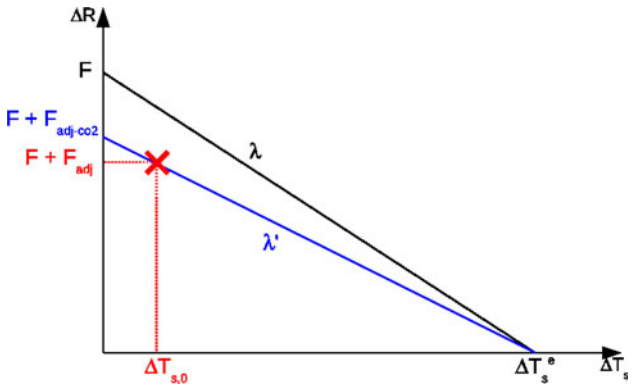

Fig. 1 Schematic representation of Eq. 1 showing the relationships between the forcings, the feedback parameters and the equilibrium global mean surface temperature when the tropospheric adjustments to CO_2 forcing are considered (in *blue*) or not (in *black*). Here, we assume that the adjustments to CO_2 are negative ($F_{adj\text{-}co2} < 0$). The intercept at $\Delta T_s = \Delta T_{s,0}$ (*red cross*) represents the adjusted radiative forcing estimated from fixed-SST experiments, in which the land surface temperature is allowed to adjust by $\Delta T_{s,0}$ to increased CO_2, while holding the SST fixed (see also Sect. 2.2)

are at least two more specific approaches that can be used to diagnose the radiative forcings and feedbacks from Eq. 5.

1. **In the case where tropospheric adjustments to CO_2 are not taken into account**, but rather included in the feedback response (e.g., in Soden and Held 2006), the changes in feedback variables X only depend on surface temperature T_s, while the dependency to CO_2 is neglected: $\Delta X \equiv \Delta X(T_s) \approx \frac{\partial X}{\partial T_s}\Delta T_s$. Eq. 5 can then be re-written as:

$$\Delta R(\mathrm{CO_2}, T_s, X(T_s)) \approx \left.\frac{\partial R}{\partial \mathrm{CO_2}}\right|_{T_s,X} \Delta \mathrm{CO_2} + \left[\left.\frac{\partial R}{\partial T_s}\right|_{\mathrm{CO_2,X}} + \left.\frac{\partial R}{\partial X}\right|_{T_s,\mathrm{CO_2}} \frac{\partial X}{\partial T_s}\right] \Delta T_s \tag{6}$$

2. **In the case where we recognize the existence of tropospheric adjustments to CO_2** while holding the SST fixed, but allowing the land surface temperature to adjust, ΔT_s can be decomposed as:

$$\Delta T_s = \Delta T_{s,0} + \Delta T_{s,\Delta SST} \tag{7}$$

where $\Delta T_{s,0}$ is the surface temperature change after CO_2 quadrupling at fixed SST and $\Delta T_{s,\Delta SST}$ is the subsequent surface temperature change when the SST varies by ΔSST.

The changes in the variables X now depend on both surface temperature and CO_2 changes as follows:

$$\Delta X \equiv \Delta X(\mathrm{CO_2}, T_s) \approx \left.\frac{\partial X}{\partial \mathrm{CO_2}}\right|_{T_s} \Delta \mathrm{CO_2} + \left.\frac{\partial X}{\partial T_s}\right|_{\mathrm{CO_2}} \Delta T_{s,0} + \left.\frac{\partial X}{\partial T_s}\right|_{\mathrm{CO_2}} \Delta T_{s,\Delta SST} \tag{8}$$

This yields for Eq. 5

$$\Delta R(\mathrm{CO_2}, T_s, X(\mathrm{CO_2}, T_s)) \approx \left[\left.\frac{\partial R}{\partial \mathrm{CO_2}}\right|_{T_s,X} + \left.\frac{\partial R}{\partial X}\right|_{T_s,\mathrm{CO_2}} \left.\frac{\partial X}{\partial \mathrm{CO_2}}\right|_{T_s}\right] \Delta \mathrm{CO_2} + \left[\left.\frac{\partial R}{\partial T_s}\right|_{\mathrm{CO_2,X}} + \left.\frac{\partial R}{\partial X}\right|_{T_s,\mathrm{CO_2}} \left.\frac{\partial X}{\partial T_s}\right|_{\mathrm{CO_2}}\right] \Delta T_{s,0} + \left[\left.\frac{\partial R}{\partial T_s}\right|_{\mathrm{CO_2,X}} + \left.\frac{\partial R}{\partial X}\right|_{T_s,\mathrm{CO_2}} \left.\frac{\partial X}{\partial T_s}\right|_{\mathrm{CO_2}}\right] \Delta T_{s,\Delta SST} \tag{9}$$

The right hand side of this equation includes the stratosphere- and troposphere-adjusted forcing to CO_2 (first row), the fast climate response to a change in land surface temperature (second row), and the climate response to the subsequent temperature change when the oceans warm (third row).

In this present study, we follow this approach to diagnose the radiative forcings and feedbacks. The next section

describes how we proceed, in practice, when we apply this methodology to CMIP5 model experiments.

2.2 Using CMIP5 experiments to diagnose radiative forcings and feedbacks

We analyze climate model outputs recently made available on the CMIP5 multi-model ensemble archive. The list of models (with their respective climate sensitivity estimated from Eqs. 22–29) considered in this study is given in Table 1.

Model outputs from a range of CMIP5 idealized experiments (described in Taylor et al. 2012) are analyzed:

1. abrupt4xCO2, a fully-coupled ocean-atmosphere simulation in which the CO_2 concentration is abruptly quadrupled and then held fixed
2. sstClim, a 30-year atmosphere-only experiment forced by a prescribed climatology of sea surface temperatures derived from fully-coupled pre-industrial simulation (piControl)
3. sstClim4xCO2, the same experiment as sstClim, except that the CO_2 concentration is abruptly quadrupled and maintained fixed for 30 years.

We compute monthly-resolved seasonal cycle using the 30-year periods of the sstClim and sstClim4xCO2 experiments and a 10-year period centered around the 130th year after the CO_2 quadrupling in abrup4xCO2. For the 3D fields, we use the data on pressure levels.

The framework described in the previous section provides the possibility of isolating the role of CO_2 and surface warming in the radiative changes associated with clouds, water vapor, albedo and temperature (Eq. 9). In the sstClim4xCO2 experiment, the atmosphere and land surface are free to respond to the change in CO_2 concentration. However, the climate feedbacks, which by definition are mediated by the global mean surface temperature change, are prevented from evolving, since the fixed-SST condition implies that $\Delta T_s \simeq 0$; actually, the small change in T_s resulting from the warming of land surfaces, $\Delta T_{s,0}$, is of the order of 0.5 K. Therefore, the fixed-SST experiments we dispose, allow us to consider the adjustments to CO_2 and land surface warming together (first two rows in Eq. 9). According to Eq. 1, the atmosphere-adjusted radiative forcing F', as defined in Eq. 12, is simply the change in the net TOA radiation fluxes between the 30-year average climate of sstClim4xCO2 and sstClim experiments (i.e., $F' = \Delta R$). As for the radiative feedbacks (third row in Eq. 9), they are investigated between the sstClim4xCO2 and abrupt4xCO2 experiments, where the CO_2 concentration is now held fixed, but the surface temperature is allowed to change as the ocean warms.

The forcing definition used in this study assumes a small warming of the climate system; the land surface warming may affect the estimates of adjustments to CO_2. Nevertheless, it has the advantage of being unambiguous and practical. Therefore, we diagnose the radiative forcing by permitting the stratospheric temperature, the troposphere and the land surface temperatures to adjust to the increased CO_2 concentration. And since the climate feedbacks are delayed by century time-scales because of the ocean's thermal inertia, it is not unreasonable to include "fast processes", such as land and sea-ice surface warming, withing the forcing rather than in the long-term climate response.

Some previous studies have attempted to devise a forcing that could capture adjustments to CO_2 without also

Table 1 Institute, model name and climate sensitivity (computed from Eqs. 22–29) of the 11 CMIP5 Global Climate Models (GCMs) considered in this study

	Model acronym	Institution	Climate sensitivity for 2 × CO_2 (in K)
1	IPSL-CM5A-LR	Institut Pierre-Simon Laplace, France	3.9
2	NorESM1-M	Norwegian Climate Center, Norway	2.7
3	MPI-ESM-LR	Max Planck Institute for Meteorology, Germany	3.7
4	INMCM4	Institute for Numerical Mathematics, Russia	1.9
5	HadGEM2-ES	Met Office Hadley Centre, United Kingdom	4.4
6	CanESM2	Canadian Centre for Climate Modelling and Analysis, Canada	3.7
7	MIROC5	Japan Agency for Marine-Earth Science and Technology, Japan	2.8
8	CCSM4	National Center for Atmospheric Research, United States	2.3
9	BNU-ESM	College of Global Change and Earth System Science, Beijing Normal University, China	4.1
10	FGOALS-s2	State Key Laboratory of Numerical Modeling for Atmospheric Sciences and Geophysical Fluid Dynamics, Institute of Atmospheric Physics, Chinese Academy of Sciences, Beijing, China	4.1
11	MRI-CGCM3	Meteorological Research Institute, Japan	2.6

capturing changes due to land surface warming. For instance, Hansen et al (2005) and Mauritsen et al. (2013) corrected the change in the net TOA radiation fluxes from fixed-SST experiments for land surface warming by evaluating $F' = \Delta R - \lambda \Delta T_{s,0}$. This was done by assuming that the global climate feedback parameter (λ) is the same in a fixed-SST experiment as in a transient experiment. However, although the global climate feedback parameter might be independent of climate state at first order, this is not necessarily true regionally nor for individual feedbacks (Boer and Yu 2003).

Another method to isolate the role of CO_2 and surface warming consists in regressing the TOA radiative imbalance of each feedback variable against the global mean temperature change (Block and Mauritsen 2013; Colman and McAvaney 2011). By doing this, the regression slopes can be understood as feedbacks and the y-intercepts as adjustments to CO_2. However, this method can sometimes lead to misleading results (e.g., the negative sea-ice albedo adjustment in Block and Mauritsen 2013) partly because different parts of the climate system may warms at different rates relative to the global mean temperature change.

Hereafter, and to ensure clarity throughout this paper, the different terms in Eq. 9 are defined as:

- the stratosphere-adjusted forcing to CO_2:

$$F = \left.\frac{\partial R}{\partial \mathrm{CO}_2}\right|_{T_s,X} \Delta \mathrm{CO}_2 \tag{10}$$

- the tropospheric adjustments to CO_2 forcing and land surface warming:

$$F_{adj} = \left.\frac{\partial R}{\partial X}\right|_{T_s,\mathrm{CO}_2} \frac{\partial X}{\partial \mathrm{CO}_2} \Delta \mathrm{CO}_2 + \left[\left.\frac{\partial R}{\partial T_s}\right|_{\mathrm{CO}_2,\mathrm{X}} + \left.\frac{\partial R}{\partial X}\right|_{T_s,\mathrm{CO}_2} \frac{\partial X}{\partial T_s}\right] \Delta T_{s,0} \tag{11}$$

- the atmosphere-adjusted forcing to CO_2 and land surface warming:

$$F' = F + F_{adj} \tag{12}$$

- the Planck feedback:

$$\lambda_p = \left.\frac{\partial R}{\partial T_s}\right|_{\mathrm{CO}_2,\mathrm{X}} \tag{13}$$

- the feedback parameter including Planck:

$$\lambda' = \lambda_p + \left.\frac{\partial R}{\partial X}\right|_{T_s,\mathrm{CO}_2} \frac{\partial X}{\partial T_s} \tag{14}$$

- In the following Sects. 2.3, 2.4 and 2.6, we describe how the tropospheric adjustments to CO_2 (Eq. 11) and the feedbacks (Eq. 14) are computed using the radiative kernel approach, and how the climate sensitivities (in Table 1) are estimated within that framework.

2.3 Estimate of adjustments

Here, the tropospheric adjustments to CO_2 and land surface warming arise, to first order, from changes in temperature (t), water vapor (wv), surface albedo (alb) and cloud (cl), which are induced by increased CO_2 and land surface warming, but without any change in sea surface temperature: $F_{adj} = \sum_x F_x + Re^f = F_t + F_{wv} + F_{alb} + F_{cl} + Re^f$ (Eq. 11), where Re^f is a residual term, usually neglected for sufficiently small climate perturbations (e.g., Soden et al. 2008). However, in large forcing experiments (e.g., $4 \times CO_2$), this residual term is sometimes too large to be ignored; this drawback of the kernel technique is discussed in more details in Sect. 2.5.

Following the same approach as for the feedback estimation (in Sect. 2.4—see also in Soden et al. 2008), all clear- and all-sky adjustment terms (except clouds) are derived using the radiative kernel technique as follows:

$$F_x = \frac{\partial R}{\partial x} \Delta x = K_x \Delta x, \tag{15}$$

where K_x is the radiative kernel. We use the same kernels as in Shell et al. (2008), the National Center for Atmospheric Research (NCAR) model's kernels for water vapor, temperature and albedo, which are made available at http://people.oregonstate.edu/~shellk/kernel.html. Each kernel, K_x, is obtained by perturbing the climate base state (with pre-industrial CO_2 concentration) by a standard anomaly δx of the corresponding climate variable x at each grid point and model level and by measuring the resulting change in TOA radiative fluxes (with separate consideration of the all- and clear-sky LW and SW radiation fluxes). See Soden et al. (2008) and Shell et al. (2008) for more details on the kernel technique.

Δx is the climate response of each variable, computed as the difference between the 30-year model predicted climate in sstClim4xCO2 and the 30-year climate of the sstClim simulation (refer to Sect. 2.2 for details on the experiments). Both K_x and Δx are functions of longitude, latitude, pressure level and are monthly means. To obtain tropospheric averages, the water vapor and temperature adjustments are vertically integrated by summing over mass-weighted model levels up to the tropopause level, which varies linearly between 300 hPa at the poles and 100 hPa at the equator. As commonly done in feedback studies, the temperature radiative response is further separated into the Planck adjustment (F_p), which is that due to a vertically uniform tropospheric warming equal the surface warming, and the lapse rate adjustment (F_{lr})

being due to deviations from uniform tropospheric warming.

The cloud adjustment is estimated by the changes in cloud radiative effect (CRE) and corrected for changes in non-cloud variables that can alter the change in CRE and lead to a biased estimate of the cloud adjustment.

$$F_{cl} = \Delta R - \Delta R^0 - \left[\sum_x (F_x - F_x^0) + (G - G^0)\right], \qquad (16)$$

where the exponent ^{0} indicates clear-sky variables, and ΔR is computed with the same experiments as Δx (i.e., between sstClim4xCO2 and sstClim). G and G^0 are the all-sky and clear-sky stratosphere-adjusted forcing computed at the tropopause, for a quadrupling CO_2, using the Laboratoire de Météorologie Dynamique (LMDz) radiation code and control climate state. $G - G^0$ is the cloud masking effect arising from changes in CO_2 concentration only, estimated at about -1.24 W m^{-2}. This yields a proportionality of cloud masking of $\frac{G-G^0}{G} \sim -0.16$, which is consistent with that reported in Soden et al. (2008).

Finally, the magnitude of the residual term Re^f (reported for each model in Table 2) is computed for clear-sky conditions (by construction, it is the same for all-sky conditions) by differencing the clear-sky TOA radiative fluxes from the sum of the clear-sky adjustment terms and clear-sky CO_2 forcing:

$$Re^f = \Delta R^0 - \left(\sum_x F_x^0 + G^0\right) = \Delta R^0 - (F_t^0 + F_{wv}^0 + F_{alb}^0 + G^0) \qquad (17)$$

In this paper, we often express this quantity in percent as: $\%Re^f = \left|\frac{Re^f}{\Delta R^0}\right| \times 100$ (also reported in Table 2 into brackets).

Vertically-integrated, global and annual mean tropospheric adjustments to CO_2 and land surface warming are shown in Table 2 for each model; multi-model ensemble-mean maps are also presented in Fig. 2. We find a relatively large negative contribution from the temperature associated with land surface warming (F_p). Clouds constitute the second most important tropospheric adjustment to CO_2; it is positive for most models, dominated by the shortwave component (F_{clsw}) and stronger over land than over the ocean (Fig. 2d, f). However, the cloud adjustment is negative over the storm track regions (Fig. 2f, and as reported in Block and Mauritsen 2013), with a greater contribution arising from the longwave component (Fig. 2e). Additional analyzes using aquaplanet experiments ('aquaControl' and 'aqua4xCO2'–not presented in the paper) show that the positive contribution from the lapse rate (over land–not shown), the water vapor (over land, Fig. 2b) and the albedo (over sea-ice, northern continental areas and semi-arid regions, Fig. 2c) are due to land surface warming rather than tropospheric adjustments to CO_2. On the other hand, cloud changes partly reflect changes in the large-scale circulation induced by the direct effect of CO_2, especially the weakening of large-scale ascending motions over ocean (Bony et al. 2013b).

These adjustment estimates may be compared with values reported in previous studies. For instance, Webb (2008)'s estimates of global cloud adjustments, obtained from the y-intercept of the regression line for ΔCRE against ΔT_s, are -1.7 ± 0.42 W m^{-2} and 0.98 ± 0.82 W m^{-2} for the LW and SW components, respectively, of an ensemble of mixed layer ocean models (note that the original $2 \times CO_2$ results have been doubled for ease of comparison with $4 \times CO_2$ results of this study). While Gregory and Webb (2008)'s and the present estimates are relatively similar for the SW component, substantial differences arise for the LW cloud adjustment. This can largely be explained by the cloud-masking effect of non-cloud variables, which is not taken into account in Gregory and Webb (2008)'s study. Our multi-model mean estimates of the adjustments in CRE are -1.42 ± 0.49 W m^{-2} and 0.93 ± 0.88 W m^{-2} for the LW and SW components, respectively, which are now very similar to Gregory and Webb (2008)'s estimates. Quantitative differences can also be found by comparing our results with those reported in Colman and McAvaney (2011), who analyzed a single model. Using the "Partial Radiative Perturbation" technique, Colman and McAvaney (2011) found that the SW cloud adjustment, estimated at ~ 1.5 W m^{-2} (scaled by 2 for comparison with $4 \times CO_2$ results of this study), is the only significant response to CO_2, while the linear regression highlights additional contributions from the LW cloud adjustment (~ -0.2 W m^{-2}, scaled by 2) and water vapor (~ -0.6 W m^{-2}, scaled by 2). The different results found by these studies highlight the sensitivity of adjustments to CO_2 to the methodology employed. Having said that, previous studies' estimates and ours remain qualitatively consistent.

2.4 Estimate of feedbacks

At first order, by neglecting interactions between variables, the feedback parameter, previously defined in Eqs. 1 and 14, is commonly split as the sum of the temperature (t), water vapor (wv), surface albedo (alb) and cloud (cl) feedback parameters (Bony et al. 2006; Soden et al. 2008), with a longwave (LW) and (SW) radiation contribution for the water vapor and cloud feedbacks. In addition, here, we consider a residual term Re^λ, which may reflect nonlinearities in the relationship between the TOA radiative flux changes and the climate responses, or more generally,

Table 2 Vertically-integrated (up to tropopause), global and annual mean of adjustments to CO_2 forcing and land surface warming (in W m^{-2}) estimated using the NCAR model's radiative kernels, for the 11 CMIP5 models used in this study, their multi-model mean and inter-model standard deviation

	F_p	F_{lr}	F_{wv}	F_{alb}	F_{clsw}	F_{cllw}	F_{cl}	$\sum_x F_x$	F'	Re^f ($\%Re^f$)
IPSL-CM5A-LR	−1.64	−0.12	0.54	0.18	2.15	−1.33	0.81	−0.21	6.48	−0.77 (10.96)
NorESM1-M	−1.72	−0.04	0.38	0.19	1.61	−0.49	1.09	−0.07	6.95	−0.49 (6.79)
MPI-ESM-LR	−1.58	0.07	0.35	0.15	1.89	−0.43	1.44	0.45	8.63	0.71 (8.39)
INMCM4	−1.45	−0.06	0.55	0.12	−0.32	0.42	0.09	−0.72	6.24	−0.54 (7.26)
HadGEM2	−1.56	0.00	0.28	0.09	1.34	−0.27	1.06	−0.12	6.99	−0.39 (5.50)
CanESM2	−1.52	−0.18	0.40	0.05	1.13	−0.04	1.07	−0.15	7.34	0.02 (0.34)
MIROC5	−1.40	−0.09	0.33	0.16	1.56	−0.66	0.89	−0.09	7.94	0.52 (6.28)
CCSM4	−1.97	0.06	0.39	0.21	1.65	−0.25	1.39	0.11	8.84	1.21 (13.80)
BNU-ESM	−1.37	−0.23	0.56	0.53	1.03	0.07	1.08	0.59	7.87	−0.21 (2.51)
FGOALS-s2	−1.15	−0.33	0.56	0.11	−0.64	0.23	−0.42	−1.22	8.05	1.80 (18.20)
MRI-CGCM3	−1.22	−0.06	0.41	0.16	0.50	0.00	0.49	−0.20	7.19	−0.10 (1.18)
For all models:										
Multi-model mean	−1.51	−0.09	0.43	0.18	1.08	−0.25	0.82	−0.15	7.50	0.16 (7.38)
Inter-model std dev	0.23	0.12	0.10	0.13	0.89	0.48	0.56	0.50	0.84	0.81 (5.38)
For the 8 models that exhibit a linear behavior (i.e., $\%Re^f < 10$):										
Multi-model mean	−1.48	−0.07	0.41	0.18	1.09	−0.17	0.90	−0.04	7.39	−0.06 (4.78)
Inter-model std dev	0.15	0.09	0.10	0.15	0.71	0.35	0.42	0.40	0.74	0.46 (3.02)

Also shown are the multi-model mean and inter-model standard deviation for the 8 models that exhibit a linear behavior in the forcing period (for which $\%Re^f < 10$; see also in Sect. 2.5). From left to right are the contributions from the Planck response to land surface warming (F_p), lapse rate (F_{lr}), water vapor (F_{wv}), albedo (F_{alb}), shortwave, longwave and net cloud components ($F_{cl\ sw}$, $F_{cl\ lw}$ and F_{cl}, respectively), the sum of all adjustments to CO_2 and land surface warming ($\sum_x F_x$), the total adjusted forcing (F') and the residual term (Re^f, expressed in W m^{-2} and $\%Re^f$ into brackets, expressed in %)

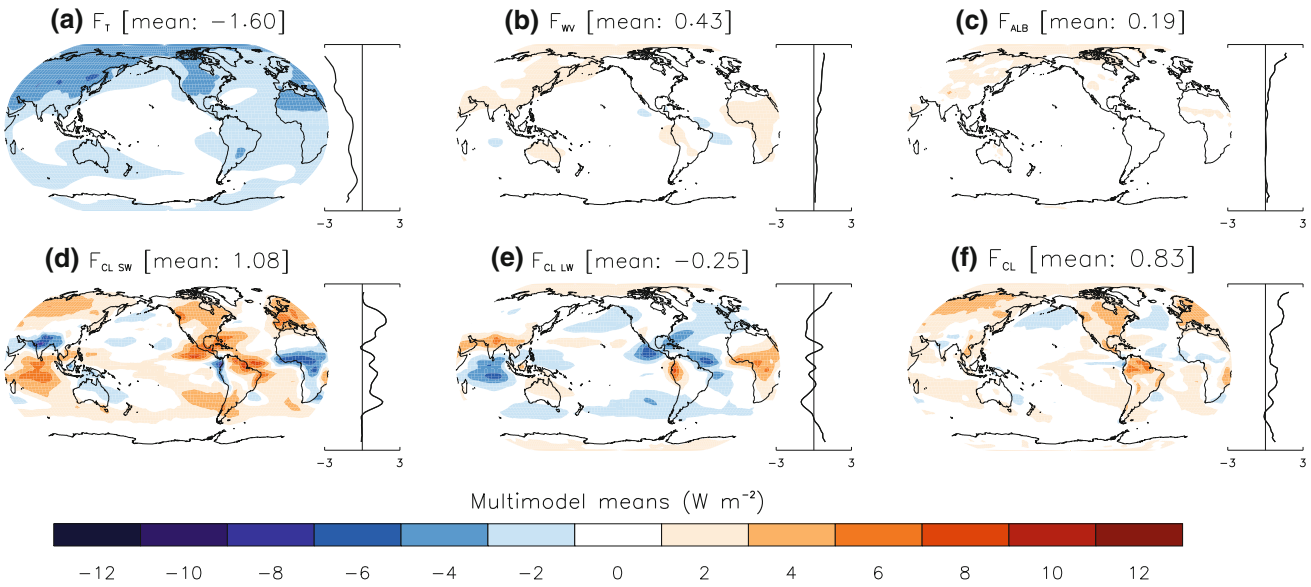

Fig. 2 Multimodel ensemble-mean maps of the tropospheric adjustments associated with temperature (**a**), water vapor (**b**), albedo (**c**) and clouds: shortwave (**d**), longwave (**e**) and net component (**f**) estimated using the NCAR model's radiative kernels and the sstClim and sstClim4xCO2 experiments. Units in W m^{-2}

limitations in the kernel approximation (as for the adjustments in Sect. 2.3): $\lambda = \sum_x \lambda_x + Re^{\lambda} = \lambda_t + \lambda_{wv} + \lambda_{alb} + \lambda_{cl} + Re^{\lambda}$.

As for the adjustments, all clear- and all-sky feedbacks (except the cloud feedback) are computed using the radiative kernel technique as follows:

$$\lambda_x = \frac{\partial R}{\partial x}\frac{\Delta x}{\Delta T_{s,\Delta SST}} \tag{18}$$

where Δx and $\Delta T_{s,\Delta SST}$ are computed by differencing the 10-year average (centered around the 130th year) model predicted climate in abrup4xCO2 from the 30-year climate of the sstClim4xCO2 simulation. By only considering the period between the abrupt4xCO2 and sstClim4xCO2 experiments, feedbacks are separated from tropospheric adjustments to CO_2, and only depend on the surface temperature change when the oceans warm. To obtain tropospheric averages, the water vapor and temperature feedbacks are vertically integrated in the same way as for the tropospheric adjustments (see Sect. 2.3). We also separate the temperature feedback into the lapse rate component (λ_{lr}) and the Planck component (λ_p).

As for the cloud feedback, we use the same approach as in Soden et al. (2008), by estimating the changes in CRE and correcting for non-cloud feedbacks.

$$\frac{\Delta CRE}{\Delta T_{s,\Delta SST}} = \frac{\Delta R - \Delta R^0}{\Delta T_{s,\Delta SST}} \tag{19}$$

$$\lambda_{cl} = \frac{\Delta CRE}{\Delta T_{s,\Delta SST}} - \sum_x (\lambda_x - \lambda_x^0), \tag{20}$$

ΔR and ΔR^0 are with the same experiments as λ_x (i.e., between abrupt4xCO2 and sstClim4xCO2), and the exponent ^{0} indicates clear-sky variables. As there is no change in forcing between these experiments, the forcing terms in Eqs. 23–25 of Soden et al. (2008) are not included in the cloud feedback calculation. Note that in Eq. 23 of Soden et al. (2008), the change in CRE is constructed from the TOA flux change residual of the clear-sky feedback factors. In doing so, they assume that the clear-sky change in TOA flux (ΔR^0) can be decomposed into the sum of clear-sky responses (i.e., $\frac{\Delta R^0}{\Delta T_{s,\Delta SST}} = \sum_x \lambda_x^0$). This might be true for small perturbations, but it is not necessarily the case when the system is forced beyond 2 × CO_2 (Jonko et al. 2012; see also in Table 3 and Sect. 2.5). Therefore, here, we compute the difference between these two terms as the residual term Re^λ, which is used to measure the accuracy for the kernel approximation of model-derived clear-sky flux changes for the abrupt4xCO2 experiment.

$$Re^\lambda = \frac{\Delta R^0}{\Delta T_{s,\Delta SST}} - \sum_x \lambda_x^0 \tag{21}$$

As for the adjustments, we also express this quantity in percent, which is defined as: $\%Re^\lambda = \left|\frac{Re^\lambda}{\Delta R^0/\Delta T_{s,\Delta SST}}\right| \times 100$ (values into brackets in Table 3).

Vertically-integrated, global and annual mean feedback parameters are shown in Table 3 for each model. For comparison, and to assess the robustness of our results, the feedbacks have also been computed using the Geophysical Fluid Dynamics Laboratory (GFDL[1]) (Soden et al. 2008) models' kernels. Both the GFDL and NCAR estimates, as well as their differences are shown in Table 3. On average over the set of models considered in this study, the two feedback calculations agree to within ±0.1 W m^{-2} K^{-1}, and the inter-model spread is the same for both models' radiative kernels. Larger uncertainties arise for the cloud components, but these are relatively small compared to the inter-model differences. These results indicate that the use of an alternative model's kernel does not alter significantly the feedback strength nor its inter-model differences. However, according to the values of the residual term Re^λ (last column in Table 3), the NCAR models' kernels reproduce the ensemble mean TOA flux changes more accurately (i.e., $Re^\lambda_{NCAR} < Re^\lambda_{GFDL}$). In the remaining of the paper, all results are therefore presented for the NCAR models' kernels only.

2.5 Clear-sky linearity test

The radiative kernel technique assumes a linear relationship between TOA radiative changes and the associated climate responses (i.e., K_x is constant, independent of models and climate states). The applicability of this method was verified for model responses to forcings of up to 2 × CO_2, but its adequacy seems reduced when the system is forced by 4 × CO_2 and beyond (Block and Mauritsen 2013; Jonko et al. 2012). In fact it has been recently shown that the radiative kernels are dependent on the control state climate and on the magnitude of the forcing (Block and Mauritsen 2013; Jonko et al. 2012).

Here, we test the applicability of the kernel method on our range of climate models, by comparing the changes in clear-sky TOA radiative fluxes derived from the model simulations and the sum of clear-sky fluxes approximated by the kernels. This analysis is performed for the zonally-averaged SW, LW and NET components of the adjustments and forcings (Fig. 3) and the feedbacks (Fig. 4), in addition of the global-averaged residual terms computed for the adjustments ($\%Re^f$, Table 2) and the feedbacks ($\%Re^\lambda$, Table 3).

The linear kernels are considered to be a useful tool for analyzes of feedbacks when the residual term is comparable to or less than 10 % relative to the simulated values (Jonko et al. 2012; Shell et al. 2008), although compensating errors could yield a small residual. We also use that criterion to test the ability of the kernels to reproduce the

[1] The GFDL model's kernels are available at http://metofis.rsmas.miami.edu/~bsoden/data/kernels.html.

Table 3 Vertically-integrated (up to tropopause), global and annual mean of feedbacks parameters (in W m^2 K^{-1}) estimated using both the GFDL and NCAR models' radiative kernels, and their multi-model mean and inter-model standard deviation

	λ_p	λ_{lr}	λ_{wv}	λ_{wv+lr}	λ_{alb}	λ_{clsw}	λ_{cllw}	λ_{cl}	$\lambda_{wv+lr+alb+cl}$	Re^{λ} (%Re^{λ})
IPSL-CM5A-LR										
GFDL	−3.29	−0.97	1.86	0.89	0.18	0.81	0.38	1.18	2.23	0.03 (1.92)
NCAR	−3.27	−0.97	1.94	0.97	0.16	0.89	0.32	1.21	2.32	−0.03 (1.57)
Diff	0.01	0.01	0.08	0.08	0.02	0.08	0.06	0.03	0.08	0.06
NorESM1-M										
GFDL	−3.19	−0.47	1.54	1.07	0.30	−0.14	0.29	0.14	1.47	0.16 (12.67)
NCAR	−3.16	−0.46	1.59	1.13	0.26	−0.04	0.23	0.18	1.53	0.07 (5.45)
Diff	0.04	0.01	0.05	0.05	0.04	0.10	0.06	0.04	0.05	0.09
MPI-ESM-LR										
GFDL	−3.27	−0.88	1.76	0.89	0.29	0.01	0.46	0.45	1.61	0.28 (22.11)
NCAR	−3.24	−0.87	1.83	0.96	0.25	0.12	0.40	0.51	1.68	0.18 (13.88)
Diff	0.03	0.00	0.07	0.07	0.05	0.11	0.06	0.05	0.08	0.11
INMCM4										
GFDL	−3.24	−0.67	1.62	0.95	0.33	−0.20	0.16	−0.05	1.20	0.06 (4.24)
NCAR	−3.20	−0.66	1.68	1.02	0.29	−0.09	0.10	0.00	1.28	−0.05 (3.22)
Diff	0.04	0.01	0.06	0.07	0.05	0.10	0.06	0.05	0.07	0.11
HadGEM2										
GFDL	−3.18	−0.55	1.49	0.94	0.29	0.00	0.41	0.39	1.57	0.51 (51.98)
NCAR	−3.14	−0.54	1.58	1.04	0.25	0.11	0.33	0.42	1.65	0.42 (43.00)
Diff	0.04	0.01	0.09	0.09	0.05	0.11	0.07	0.04	0.08	0.09
CanESM2										
GFDL	−3.23	−0.64	1.67	1.03	0.32	−0.21	0.74	0.52	1.83	0.19 (15.18)
NCAR	−3.18	−0.64	1.72	1.07	0.26	−0.10	0.68	0.57	1.87	0.10 (8.38)
Diff	0.04	0.01	0.05	0.04	0.05	0.11	0.06	0.05	0.04	0.08
MIROC5										
GFDL	−3.22	−0.66	1.68	1.02	0.36	−0.22	0.28	0.04	1.38	0.10 (8.50)
NCAR	−3.21	−0.63	1.74	1.11	0.33	−0.11	0.21	0.08	1.47	0.03 (2.36)
Diff	0.01	0.03	0.07	0.09	0.04	0.11	0.07	0.04	0.09	0.07
CCSM4										
GFDL	−3.18	−0.44	1.48	1.05	0.40	−0.27	−0.14	−0.42	1.00	−0.26 (18.51)
NCAR	−3.14	−0.44	1.55	1.11	0.32	−0.13	−0.22	−0.36	1.04	−0.31 (21.85)
Diff	0.05	0.00	0.07	0.06	0.08	0.15	0.09	0.06	0.04	0.05
BNU-ESM										
GFDL	−3.15	−0.22	1.39	1.17	0.48	−0.17	0.28	0.09	1.70	0.28 (39.76)
NCAR	−3.10	−0.23	1.43	1.20	0.39	−0.02	0.22	0.18	1.73	0.20 (28.58)
Diff	0.05	0.01	0.04	0.03	0.09	0.15	0.06	0.09	0.03	0.08
FGOALS-s2										
GFDL	−3.20	−0.53	1.73	1.20	0.37	−0.37	0.28	−0.10	1.43	0.60 (122.58)
NCAR	−3.16	−0.52	1.77	1.25	0.32	−0.26	0.21	−0.06	1.47	0.53 (108.70)
Diff	0.04	0.01	0.04	0.05	0.06	0.11	0.07	0.05	0.03	0.07
MRI-CGCM3										
GFDL	−3.22	−0.61	1.53	0.92	0.37	0.21	−0.00	0.21	1.46	0.11 (8.72)
NCAR	−3.17	−0.60	1.60	1.00	0.32	0.32	−0.09	0.23	1.51	0.06 (4.83)
Diff	0.05	0.01	0.07	0.07	0.05	0.11	0.09	0.02	0.04	0.05
Multimodel mean and intermodel standard deviation										

Table 3 continued

	λ_p	λ_{lr}	λ_{wv}	λ_{wv+lr}	λ_{alb}	λ_{clsw}	λ_{cllw}	λ_{cl}	$\lambda_{wv+lr+alb+cl}$	Re^{λ} ($\%Re^{\lambda}$)
GFDL	−3.22 (0.04)	−0.60 (0.21)	1.61 (0.14)	1.01 (0.11)	0.34 (0.08)	−0.05 (0.33)	0.28 (0.23)	0.22 (0.42)	1.54 (0.32)	0.19 (0.23)
NCAR	−3.18 (0.05)	−0.60 (0.20)	1.68 (0.14)	1.08 (0.09)	0.28 (0.06)	0.06 (0.32)	0.22 (0.24)	0.27 (0.41)	1.59 (0.33)	0.11 (0.23)
Diff	0.04	0.00	0.06	0.07	0.05	0.11	0.07	0.05	0.06	0.08
Multi-model mean and inter-model standard deviation for the 6 models that exhibit a linear behavior (i.e., $\%Re^{\lambda} < 10$)										
GFDL	−3.23 (0.03)	−0.67 (0.17)	1.65 (0.12)	0.98 (0.07)	0.31 (0.07)	0.04 (0.41)	0.31 (0.25)	0.34 (0.45)	1.60 (0.37)	0.11 (0.06)
NCAR	−3.20 (0.04)	−0.66 (0.17)	1.71 (0.13)	1.05 (0.06)	0.27 (0.06)	0.14 (0.40)	0.24 (0.26)	0.38 (0.45)	1.66 (0.37)	0.03 (0.06)
Diff	0.03	0.01	0.06	0.07	0.04	0.10	0.07	0.04	0.06	0.08

Also shown for each model, with the same units, is the difference in feedbacks' strength between the two models' kernels. The magnitude of the residual term is also presented (Re^{λ}, expressed in W m^{-2} K^{-1} and $\%Re^{\lambda}$ into brackets, expressed in %), as well as the multi-model mean and inter-model standard deviation for the 6 models that exhibit a linear behavior in the feedback period (for which $\%Re^{\lambda} < 10$; see also in Sect. 2.5). Note that the multi-model means and inter-model standard deviations of the residual term is only expressed in W m^{-2} K^{-1}

global-averaged simulated flux changes in the fixed-SST and the abrupt4xCO2 experiments.

For both the adjustments and the feedbacks, there is a good agreement in the spatial structure of the multi-model mean simulated changes in clear-sky fluxes (black lines) compared to those estimated using the kernels (red lines). However, the magnitude and the inter-model spread of model-derived flux changes are not always well reproduced by the kernels.

For the adjustments (top part of Fig. 3a–c), the NET TOA clear-sky radiative imbalance is positive everywhere and dominated by the LW forcings. A small positive contribution also arises from the SW component between 60°N and 90°N, where there are surface albedo changes due to melting snow and sea-ice as land surfaces warm (Fig. 2c). Values of the residual term for the adjustments, reported for each model in Table 2 ($\%Re^{f}$), tend to be relatively small, except for three models for which $\%Re^{f}$ is just above 10 % (IPSL-CM5A-

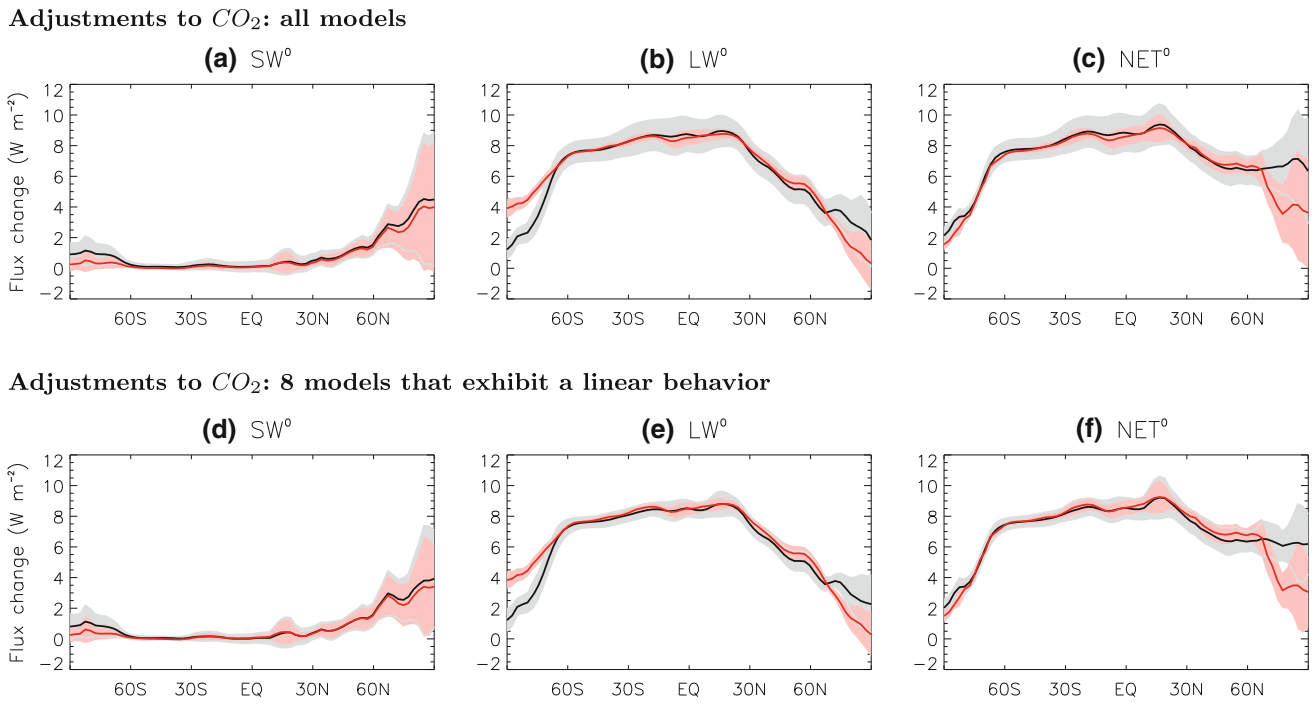

Fig. 3 Multi-model mean (*solid lines*) and inter-model standard deviation (*shading*) for the change in clear-sky TOA fluxes as derived from model output (ΔR^0, in *black*), and for the sum of clear-sky adjustments and forcings derived from the NCAR model's kernels ($\sum_x F_x^0 + G^0$, in *red*). Zonally-averaged fluxes in W m^{-2}. **a–c** show the SW, LW and NET components for all models. **d–f** is for the 8 models that exhibit a linear behavior (for $\%Re^{f} < 10$ in Table 2)

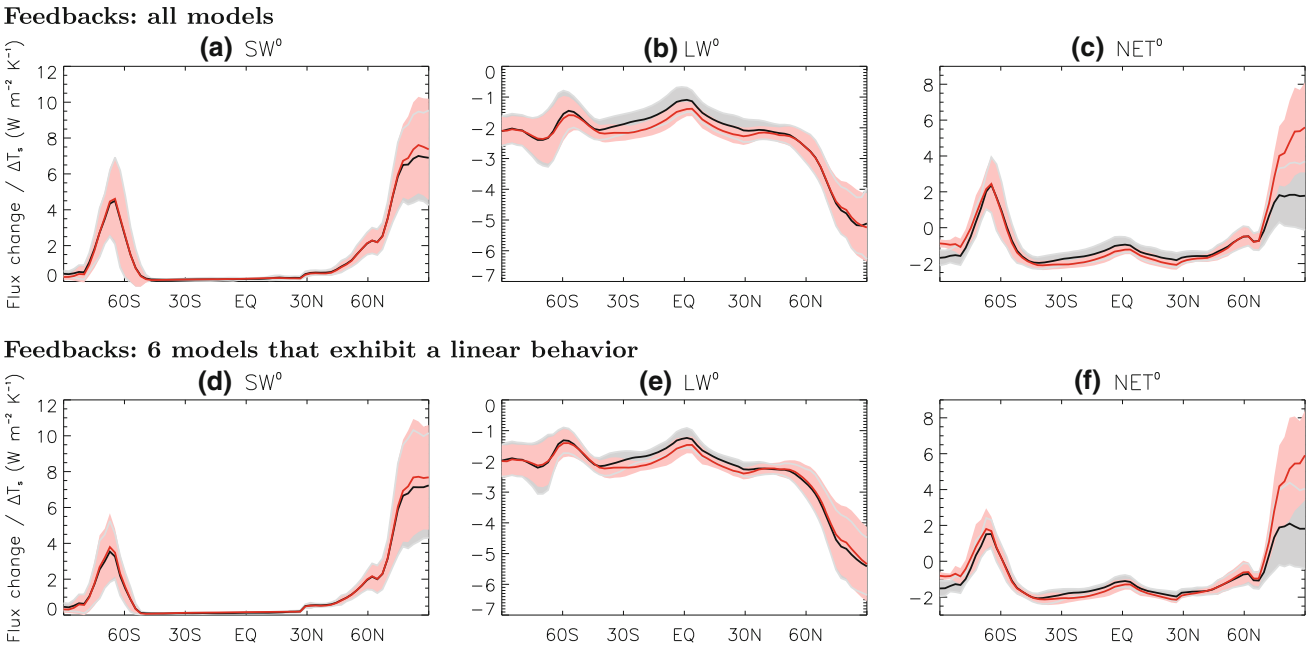

Fig. 4 Same as Fig. 3 but for the feedbacks. TOA flux changes derived from model output have been normalized by $\Delta T_{s,\Delta SST}$ for comparison with the feedbacks. Units are W m^{-2} K^{-1}. **a–c** is the SW, LW and NET components for all models, and **d–f** is for the 6 models that exhibit a linear behavior (for $\%Re^f < 10$ in Table 3)

LR, CCSM4 and FGOALS-s2). The ability of the kernels to reproduce the global averaged model-derived flux changes, arises, however, from hemispheric compensating errors in the LW component: the kernels systematically overestimate the model-derived flux changes between 60°S and 90° S, while over the Arctic the simulated flux changes are slightly underestimated (Fig. 3b).

For the feedbacks (top part of Fig. 4a–c), the NET clear-sky flux changes are negative everywhere and dominated by the LW component, except over the Arctic and Southern Ocean because of strong SW flux changes associated with decreased surface albedo. There is a systematic difference over the poles, where the net radiative changes, computed using the kernels, are overestimated, while elsewhere they rather tend to be slightly underestimated (Fig. 4c). In most models the kernels overestimate the model-derived SW flux change over the Arctic and Southern Ocean (Fig. 4a). As for the changes in LW flux, the kernels generally underestimate the model-derived values between 30°S and 30°N (Fig. 4b), while no clear tendency emerges at middle and high latitudes because of a large inter-model spread in the differences between the kernel- and the model-derived changes (not shown). We find that the linear kernel analysis is applicable to six models only for the feedback calculation, namely IPSL-CM5A-LR, NorESM1-M, INMCM4, CanESM2, MIROC5 and MRI-CGCM3 (for which $\%Re^{\lambda} < 10$ in Table 3).

The results presented in Figs. 3 and 4 also show that the kernel method tends to underestimate the inter-model standard deviation of the changes in clear-sky fluxes (compare the width of red and grey shadings; grey is wider than red shading). The bias introduced by the kernel method essentially affects the clear-sky LW component over the tropics and the mid-latitudes (Figs. 3b, 4b).

We repeated the calculations shown in Figs. 3a–c and 4a–c, but by only using the models that behave linearly, for which $\%Re^f < 10$ and $\%Re^{\lambda} < 10$, respectively, and we find that the inter-model spread of kernel-derived clear-sky flux changes is now in good agreement with that of model-derived values (red and grey shadings have similar width in Figs. 3d–f, 4d–f).

Finally, large deviations from linearity are found in the feedbacks for MPI-ESM-LR (14 %), HadGEM2 (43 %), CCSM4 (22 %), BNU-ESM (29 %), FGOALS-s2 (109 %), and in the forcings for IPSL-CM5A-LR (11 %), CCSM4 (14 %) and FGOALS-s2 (18 %), which call into question the robustness of the linear assumption in the calculation of feedbacks and forcings for those models. Given the results presented in this section, the kernel method might have quantitative limitations for these models that exhibit a nonlinear behavior, but is qualitatively consistent with model-derived analysis. In the remaining of the paper, we therefore present our analysis using all models, but to ensure robustness in our interpretations, we verify our conclusions by restricting our analysis to the models that exhibit a linear behavior in the forcing or feedback calculation.

2.6 Relative contributions of feedbacks and adjustments to climate sensitivity

Here, we follow the methodology employed in Dufresne and Bony (2008) to decompose the contributions of the different feedbacks and adjustments to the equilibrium global temperature change ΔT_s^e.

The energy balance in Eq. 9, combined with Eqs. 10–21, separating the Planck feedback from the non-Planck feedbacks and normalizing by the Planck feedback, can be rewritten as:

$$\Delta T_{s,\Delta SST} = \frac{-1}{\lambda_p}\left[F + F_{adj} - \Delta R + \left(\sum_{x\neq p}\lambda_x + Re^{\lambda}\right)\Delta T_{s,\Delta SST}\right] \tag{22}$$

At equilibrium, when $\Delta R = 0$, it becomes:

$$\Delta T^e_{s,\Delta SST} = \frac{-1}{\lambda_p}\left[F + F_{adj} + \left(\sum_{x\neq p}\lambda_x + Re^{\lambda}\right)\Delta T^e_{s,\Delta SST}\right] \tag{23}$$

with $\Delta T^e_{s,\Delta SST} = \frac{F'}{\lambda'}$ (by substituting F and λ for F' and λ' in Eq. 2).

Finally, because we consider the radiative changes due to land surface warming as part of the forcings rather than of the feedbacks (which therefore act to reduce the effective forcing—see Fig. 1), we must add to the equilibrium global temperature change when the ocean warms, in Eq. 23, the contribution from the warming of land surfaces $\Delta T_{s,0}$. Therefore, the total equilibrium global temperature change is defined as:

$$\begin{aligned}\Delta T_s^e &= \frac{-1}{\lambda_p}\left[F + F_{adj} + \left(\sum_{x\neq p}\lambda_x + Re^{\lambda}\right)\Delta T^e_{s,\Delta SST}\right] + \Delta T_{s,0}\\ &= \Delta T^e_{s,\Delta SST} + \Delta T_{s,0}\end{aligned} \tag{24}$$

From Eq. 24, we define:

- the Planck response associated with the stratosphere-adjusted forcing (F):

$$\Delta T_{s,F} = -\frac{F}{\lambda_p}, \text{ as in Eq.4 of Dufresne and Bony (2008)} \tag{25}$$

- the Planck response associated with all the tropospheric adjustments to CO_2 forcing and land surface warming:

$$\Delta T_{s,F_{adj}} = -\frac{F_{adj}}{\lambda_p} + \Delta T_{s,0} \tag{26}$$

- More explicitly, this term includes direct adjustments to CO_2 and adjustments to land surface warming associated with temperature, water vapor, albedo and clouds, the residual for the forcings (Re^f), and the actual small warming of land surfaces ($\Delta T_{s,0}$, largely compensated by the radiative cooling of the Planck component F_p).
- the temperature change associated with each feedback parameter x, in response to the atmosphere-adjusted forcing F':

$$\Delta T_{s,x} = -\frac{\lambda_x}{\lambda_p}\Delta T^e_{s,\Delta SST} \tag{27}$$

- and the temperature change associated with the feedback residual term Re^{λ} :

$$\Delta T_{s,Re} = -\frac{Re^{\lambda}}{\lambda_p}\Delta T^e_{s,\Delta SST} \tag{28}$$

such that:

$$\Delta T_s^e = \Delta T_{s,F} + \Delta T_{s,F_{adj}} + \sum_{x\neq p,adj}\Delta T_{s,x} + \Delta T_{s,Re}, \tag{29}$$

3 Decomposition of climate sensitivity estimates from CMIP5 models

The climate sensitivity estimates of the 11 models considered in this study (as computed from Eqs. 22–29 and reported in Table 1) range between 1.9 and 4.4° for a doubling of CO_2 concentration. This range is similar (although slightly lower) than that of CMIP3 (Randall et al. 2007) and than that of CMIP5 diagnosed by Andrews et al. (2012) using a different methodology. Actually, the differences between Andrews et al. (2012)'s estimates and ours remain within ±5 % for the 7 models that are analyzed in both studies, while one model only (INMCM4) exhibits a larger difference between the two methodologies (9.5 % difference). These results are therefore rather promising given all the uncertainties involved in estimating the climate sensitivity of models, and the very different nature of the two methodologies.

We now analyze the decomposition of equilibrium temperature changes into forcing and feedback terms, as described in Sect. 2.6, for the 11 models (in Table 1). In addition, each contribution to the equilibrium temperature change is separated into three different regions: the tropics (between 30°S and 30°N), the mid-latitudes (between 30° and 60° in each hemisphere) and the poles (between 60° and 90° in each hemisphere). Each regional contribution is weighted by its respective surface area, so that the sum of all regions equals the global value.

3.1 Multi-model mean analysis

The multi-model mean of the equilibrium temperature change ΔT_s, decomposed into regional contributions, feedbacks and into the Planck response of stratosphere-adjusted forcing and adjustments, is shown in Fig. 5a. On average over the set of models considered in this study,

43 % of the global warming is associated with the direct response to CO_2 forcing (36 % for the stratosphere-adjusted forcing and 7 % for the adjustments), and 57 % from the feedbacks: 32 % of the warming arises from the combined water vapor + lapse rate (hereafter, WV+LR), 10 % from clouds, 8 % from surface albedo and 7 % from the feedback residual term. When we restrict our analysis to the 6 models for which the residual term is lower than 10 % (in Table 3), the contribution to ΔT_s arising from clouds increases up to 14 % and that of the residual term becomes less than 3 %, while the contribution from the other components changes by at most 2 % (not shown). This suggests that errors introduced by the radiative kernels in the calculation of feedbacks mainly affect the cloud component, and lead to an underestimation of the multi-model mean temperature change that results from the cloud feedback.

These results are qualitatively similar to those reported by Dufresne and Bony (2008). However, quantitative differences may arise from the fact that cloud adjustments are now included in the forcing term rather than in the feedback term. Indeed, cloud adjustment to CO_2 is generally positive, except for CCSM4 (Table 2), and the estimated cloud feedback is reduced; the multi-model mean cloud feedback is about 33 % weaker (see Sect. 4.2, where different measures of the cloud feedback are compared). As demonstrated in Sect. 2.1, if the climate sensitivity is not affected by the methodology (this is verified with an uncertainty to within ±3 %), the feedback parameter, however, is (according to the relation in Eq. 4 and Fig. 1). The negative total feedback parameter is enhanced by 11 % (not shown) compared to the previous methodology (Eq. 6).

It is interesting to mention that the differences between the adjusted feedback parameters (calculated between sstClim4xCO2 and abrupt4xCO2) and the non-adjusted feedbacks (calculated between sstClim and abrupt4xCO2) are rather small for the non-cloud feedbacks and for the feedback residual term; the multi-model mean difference is 2 % for the temperature and albedo feedbacks, 6 % for the water vapor feedback and 5 % for the residual term (not shown). This suggests that the positive cloud adjustment (in Table 2) is the main component that can alter the feedback parameter, and that the non-cloud adjustments associated with temperature, water vapor and albedo seem to be better understood as responses to land surface warming.

It appears in Fig. 5a (left bar) that each latitude belt contributes to global ΔT_s in proportion to its area: the tropical contribution is ~50, ~35 % arises from the mid-latitudes and ~15 % from polar regions. Note however that regional contributions to the inter-model spread are not necessarily proportional to their area extent.

3.2 Feedback parameters

The amplitude of ΔT_s associated with the Planck response (i.e., of stratosphere-adjusted forcing + adjustments, obtained by summing Eqs. 25, 26) and the feedbacks is shown in Fig. 5b. The contributions from the different regions is also represented for each component, and the sum of all regions (represented by the black dots) corresponds to the global climate sensitivity estimate (also reported in Table 1).

For all models, the contribution to ΔT_s from the Planck response to forcing is the greatest in the tropics and the smallest over the poles. A similar tendency is observed for the clouds, the residual term and the combined water vapor + lapse rate feedback. However, as expected from sea-ice loss and snow melt with rising temperatures, the albedo feedback is the largest over polar regions.

Inter-model differences occur for each feedback, but those associated with cloud feedbacks are the largest (Fig. 5b). As a result, the spread of climate sensitivity is primarily driven by the spread of cloud feedbacks, especially tropical cloud feedbacks. This is confirmed by the comparison of the normalized inter-model standard deviation associated with each feedback and each region (Fig. 6a for all models and Fig. 7a for the 6 models with $\%Re^{\lambda} < 10$), and by the inter-model regression of the feedbacks against the global mean temperature change (Fig. 8). These maps of regression slopes indicate the feedbacks and the regions the most strongly associated with the inter-model spread in climate sensitivity; positive (negative) values means that the global mean climate sensitivity is positively (negatively) correlated with the local feedback parameter. Figure 8f shows that high sensitivity models tend to have strong positive cloud feedbacks in the tropics, with contributions from the SW component in subsidence zones (Fig. 8d), and from the LW component in convective regions (Fig. 8e). Moreover, although at a lesser extent, high sensitivity models have a positive cloud feedback over the oceanic basins in the mid-latitudes, associated with a reduced cloud-albedo effect in the storm track regions (Fig. 8d).

Inter-model differences in cloud feedbacks represent about 55 % the standard deviation of climate sensitivity in Fig. 6a. This estimate is substantially reduced as compared to the "70 %" reported by Dufresne and Bony (2008), and this is not due to the fact that tropospheric adjustments to CO_2 are now included in the forcing term rather than in the feedback term. It is, however, highly sensitive to the feedback residual term (which contributes for 34 % to the inter-model standard deviation in ΔT_s in Fig. 6). When we restrict our analysis to the 6 models that have a small residual term (i.e., $\%Re^{\lambda} < 10$ in Table 3), its contribution

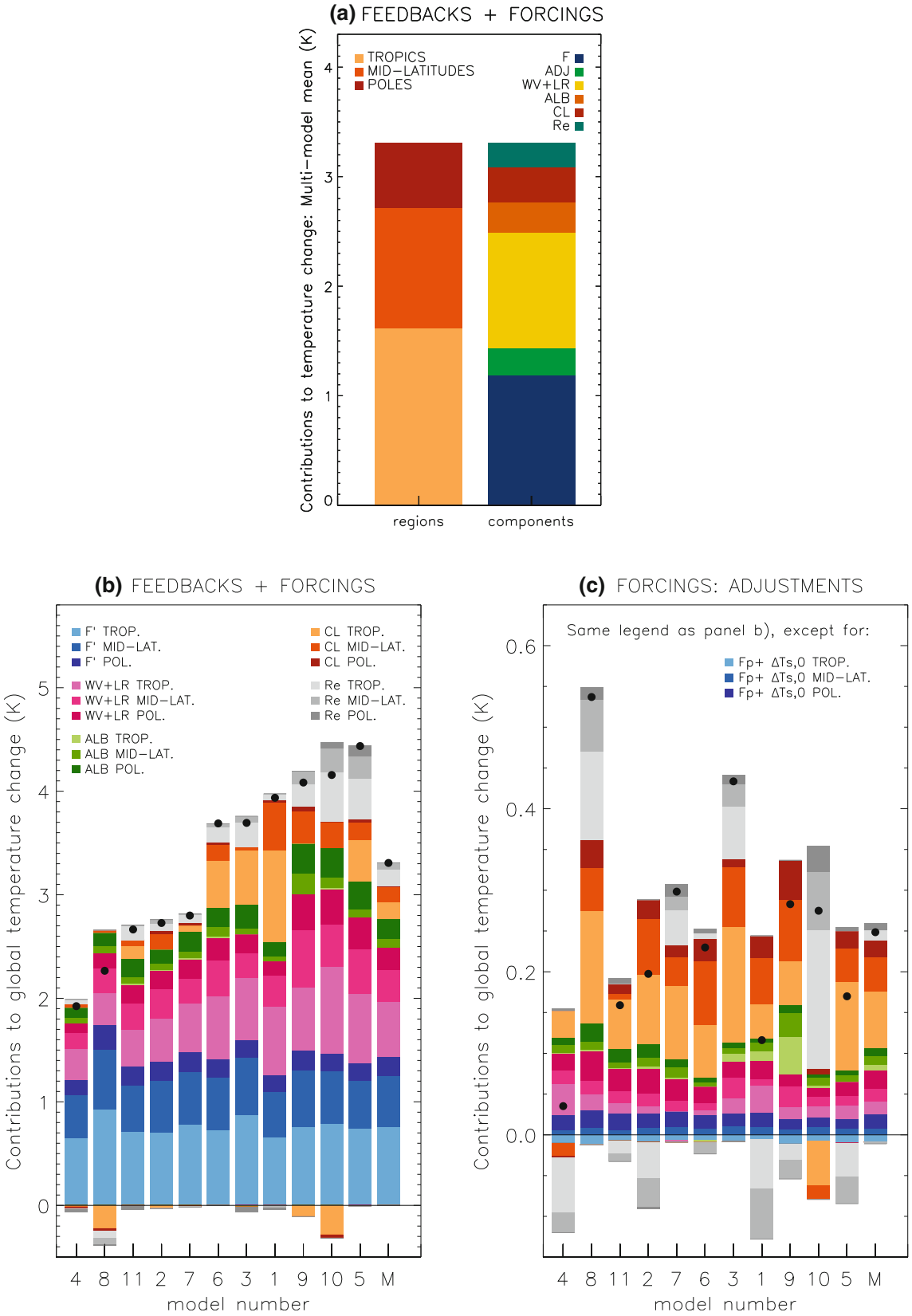
(a) FEEDBACKS + FORCINGS
Contributions to temperature change: Multi−model mean (K)
TROPICS
MID−LATITUDES
POLES
F
ADJ
WV+LR
ALB
CL
Re
regions
components
(b) FEEDBACKS + FORCINGS
Contributions to global temperature change (K)
F' TROP.
F' MID−LAT.
F' POL.
WV+LR TROP.
WV+LR MID−LAT.
WV+LR POL.
ALB TROP.
ALB MID−LAT.
ALB POL.
CL TROP.
CL MID−LAT.
CL POL.
Re TROP.
Re MID−LAT.
Re POL.
4 8 11 2 7 6 3 1 9 10 5 M
model number
(c) FORCINGS: ADJUSTMENTS
Same legend as panel b), except for:
Fp+ ΔTs,0 TROP.
Fp+ ΔTs,0 MID−LAT.
Fp+ ΔTs,0 POL.
Contributions to global temperature change (K)
4 8 11 2 7 6 3 1 9 10 5 M
model number

◀ **Fig. 5** **a** multi-model mean of the climate sensitivity estimate ΔT_s, separated into regional contributions from the tropics (between 30°S and 30°N), the mid-latitudes (between 30°and 60° in each hemisphere) and the poles (between 60° and 90° in each hemisphere) (*left*) and into its different components, including the Planck response to stratosphere-adjusted forcing (F, Eq. 25), the Planck response to the adjustments to CO_2 forcing and land surface warming (ADJ, Eq. 26), the combined water vapor + lapse rate (WV+LR), the albedo (ALB), the cloud (CL) feedbacks (Eq. 27) and the feedback residual term (Re^{λ}, Eq. 28) (*right*). **b** climate sensitivity estimates (as indicated by the *black dots*) associated with the Planck response to the stratosphere-adjusted forcing and the adjustments (F', in *blue*–obtained by summing Eqs. 25 and 26), the combined water vapor + lapse rate feedback (WV+LR, in *purple*), the albedo feedback (ALB, in *green*), the net could feedback (CL, in *red*) and the feedback residual term (Re, in *grey*), computed for each of the 11 models listed in Table 1. $\Delta T_{s,F} + \Delta T_{s,F_{adj}}$, $\Delta T_{s,x}$ and $\Delta T_{s,Re}$'s are also decomposed into the three different regions: the tropics (*light shading*), the mid-latitudes (*medium shading*) and the poles (*dark shading*). **c** global mean surface temperature change (as indicated by the *black dots*) associated with the Planck response to land surface warming ($\Delta T_{s,F_p}$) + $\Delta T_{s,0}$ (*blue*), the adjustments for the combined water vapor + lapse rate (*purple*), the albedo (*green*), the net could adjustments (*red*) and the residual term (*grey*). The models are sorted according to increasing ΔT_s, and model numbers correspond to the listing in Table 1. The last column (*M*) in panels (b) and (c) correspond to the multi-model mean for the feedbacks and adjustments, respectively. Note the different scales of the temperature change (*y*-axis) among each panel

to the inter-model standard deviation in ΔT_s drops to only 10 %, while that of the cloud feedbacks increases up to 70 % (Fig. 7a). Therefore, the limitations in the kernel approximation not only affect the magnitude of the cloud-related temperature change, as shown previously, but also lead to an underestimation of cloud-induced inter-model spread in climate sensitivity. The tropics is clearly the region where the spread in cloud feedbacks is the largest (48 %), followed by the mid-latitudes (23 %) and the poles (3 %). If the temperature spread resulting from the cloud feedback is underestimated by the kernel method, that associated with the non-cloud feedbacks, however, is overestimated (compare Figs. 6a, 7a). The contribution of WV+LR to the inter-model spread in climate sensitivity, which is the second most important source of spread in ΔT_s, is 25 % weaker for the models that have a small feedback residual term (30 % in Fig. 7a and 40 % in Fig. 6a). For this component, the spread also primarily originates from the tropics, and is mainly driven by the water vapor feedback (Fig. 8b), while the lapse rate feedback tends to be more strongly associated (and anti-correlated) with the temperature spread over the middle and high latitudes (Fig. 8a).

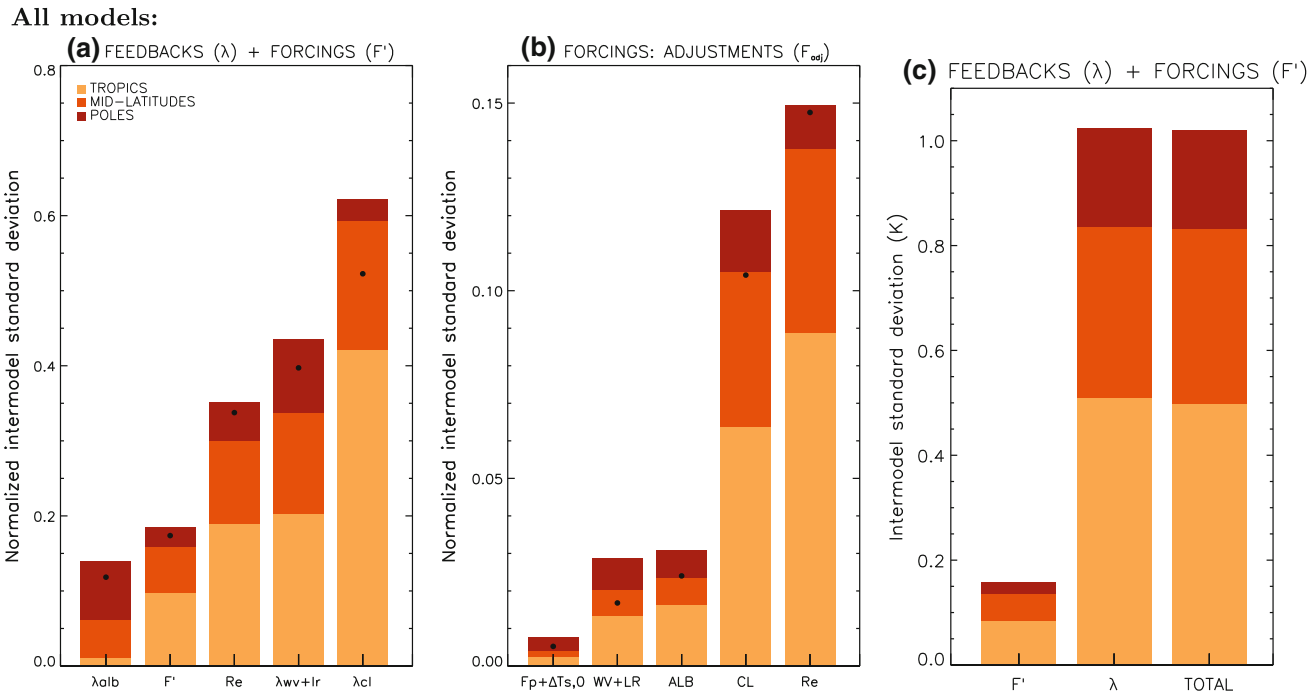

Fig. 6 **a** Inter-model standard deviation of climate sensitivity estimates associated with the atmosphere-adjusted forcing (which includes the Planck response to the stratosphere-adjusted forcing and to the adjustments) and the feedbacks in each region, normalized by the inter-model standard deviation of ΔT_s (no units). Note that for this metrics, the contributions from the different regions are not additive, and the normalized inter-model standard deviation of ΔT_s over the globe is reported as *black dots*. **b** same as (**a**), but for the Planck response to the adjustments only. **c** Inter-model standard deviation of climate sensitivity estimates (in Kelvin) associated with the atmosphere-adjusted forcing (which includes the Planck response to the stratosphere-adjusted forcing and to the adjustments) and the feedbacks (λ). The last bar (TOTAL) is the inter-model standard deviation of ΔT_s associated with both the forcing and the feedbacks. Note the different scales and units on the *y*-axis among each panel. Note also that, unlike it appears in panel (c), the regional contributions to the inter-model standard deviation are not necessarily proportional to their area extent

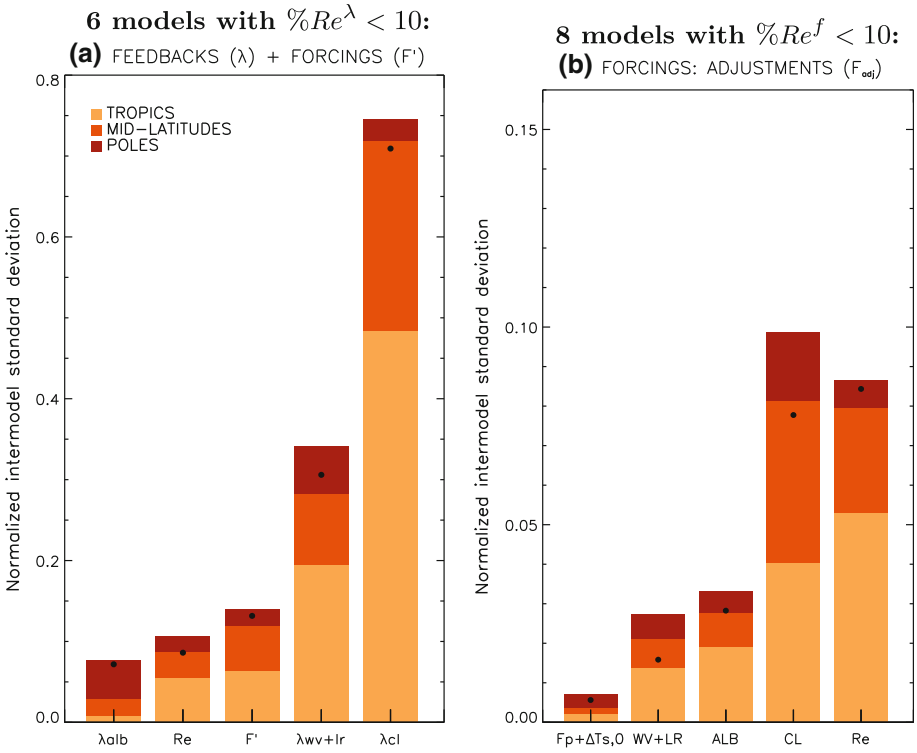

Fig. 7 **a** Same as Fig. 6a, but for the 6 models for which the residual for the feedbacks $\%Re^{\lambda} < 10$ (see Table 3). **b** Same as Fig. 6b, but for the 8 models for which the residual for the adjustments $\%Re^{f} < 10$ (see Table 2)

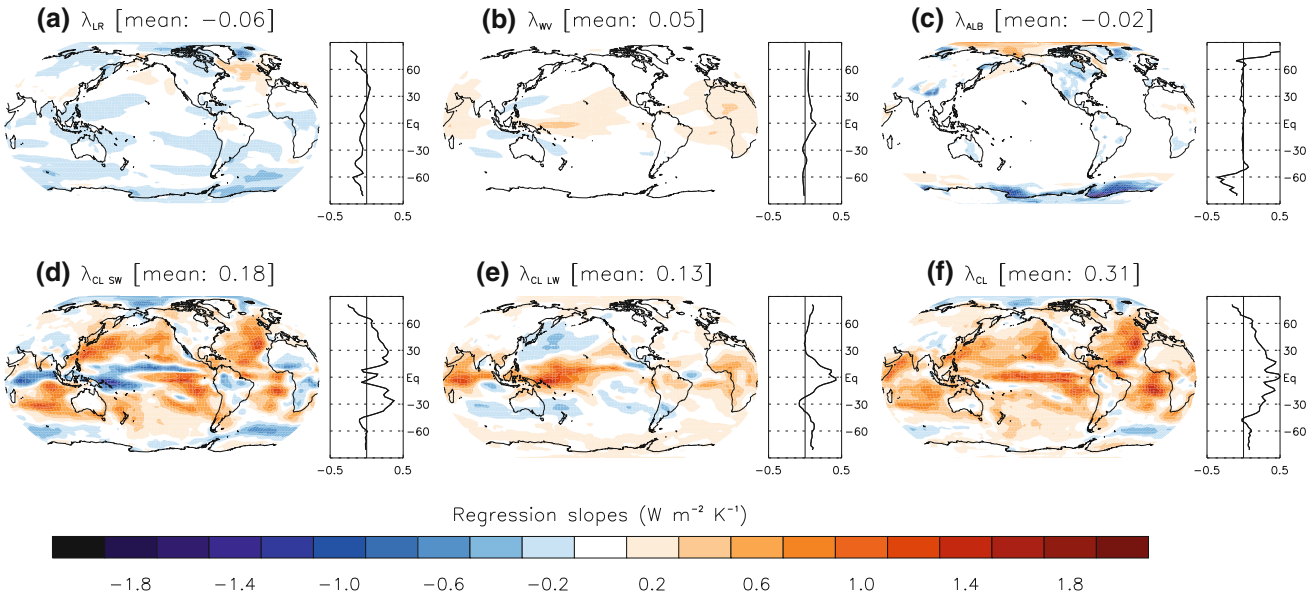

Fig. 8 Inter-model regression slopes of the lapse rate (**a**), water vapor (**b**), albedo (**c**) and cloud (SW in **d**; LW in e; NET in **f**) feedbacks against the global mean surface temperature change for the 11 models considered in this study and reported in Table 1. Large values indicate the regions where the feedbacks are the most strongly associated with the inter-model spread in climate sensitivity. Positive (negative) values means that the global mean climate sensitivity is positively (negatively) correlated with the local feedback parameter

The spread of climate sensitivity arising from the direct response to CO_2 (i.e., stratosphere-adjusted forcing + adjustments) is less than 15 % in Fig. 7a, with the largest contributions in the tropics and the mid-latitudes (6 % of ΔT_s in each region). The temperature spread resulting from the surface albedo is the smallest ($<10\%$ in Fig. 7a), with the largest contribution over polar regions. This also appears in Fig. 8c, where the global mean surface temperature change is positively associated with the surface albedo feedback over the Arctic region, while both measures are anti-correlated over Southern Ocean.

3.3 Adjustments to CO_2 forcing and land surface warming

A similar analysis is performed for the Planck response to tropospheric adjustments associated with water vapor, lapse rate, surface albedo, clouds, and the residual for forcings (Figs. 5c, 6b, 7b). Recall also from Eq. 26 that there is a contribution from surface temperature, which includes the actual warming of land surfaces ($\Delta T_{s,0}$) and the Planck response ($\Delta T_{s,F_p}$). We consider those two components together rather than each term individually, because they are strongly correlated and largely offset each other ($\Delta T_{s,F_p} + \Delta T_{s,0}$, in Fig. 5c).

The sum of all adjustments produces a small warming ($\Delta T_{s,F_{adj}}$), ranging between 0.04 and 0.54 K (black dots in Fig. 5c). No correlation appears between the spread associated with adjustments and that associated with feedbacks. On average over the 11 models, the largest adjustment arises from the clouds (53 % of $\Delta T_{s,F_{adj}}$), followed by the WV+LR (22 %), the albedo (11 %), the residual term (8 %) and the contribution from land surface warming (6 %). When we only consider the 8 models that have a small residual term (i.e., $\%Re^{f<10}$ in Table 2), there is an increased contribution from the clouds (up to 64 % of $\Delta T_{s,F_{adj}}$), which tends to be compensated by a decreased contribution from the residual term, while the other components remain fairly similar (as also seen in Table 2). Therefore, similarly to the feedbacks, the results indicate that errors associated with the kernel method pertain mainly to the cloud component and lead to an underestimation of the multi-model mean cloud-induced temperature change.

Although the multi-model mean of the cloud response is the greatest, the residual term constitutes the largest spread in the amplitude and in the sign of the adjustments (Fig. 5c). The contribution of Re^f to the inter-model standard deviation in ΔT_s is also the largest among all adjustments, especially in the tropics (Fig. 6b), and this result remains robust when we restrict the analysis to the 8 models with $Re^{f<10}$ (Fig. 7b). Having said that, the residual term for the forcings contribute only 9 % of the total spread (Fig. 7b), which is less than that of any individual feedback parameter alone (Fig. 7a). Hence, the inter-model spread of climate sensitivity arises primarily from the spread of feedbacks rather than adjustments.

The spread resulting from the cloud adjustment is nearly 8 % of the inter-model difference in ΔT_s (Fig. 7b). The tropics contribute the most to the global response in clouds (35 % of the multi-model mean for the 8 models with $\%Re^{f<10}$), but it is not the principal source of spread. The tropics and the mid-latitudes contribute almost equally to the temperature spread (Fig. 7b), while the polar regions constitute the smallest spread.

The WV+LR response is weaker than that of the net cloud adjustment (Fig. 5c), with polar regions contributing the most to the global response because of a positive lapse rate response associated with a larger surface warming in these areas, and a relatively small water vapor response in warm regions. Over the tropics and the mid-latitudes the WV+LR adjustment is similar, with a weak but positive (negative) WV (LR) response consistent with the slight land and tropospheric warmings associated with increased CO_2 concentration. Although the greatest WV+LR adjustment is over polar regions, the largest spread is, as for the feedbacks, over the tropics (in Figs. 6b, 7b).

The amplitude of adjustment associated with the surface albedo is small, each region contributing equally to the global response, but its contribution to the spread in ΔT_s is comparable to that of the WV+LR adjustment (in Figs. 6b, 7b), although slightly greater in the tropics and the mid-latitudes. The high tropical surface albedo response (e.g., for models 1 and 9 in Fig. 6b) arises from semi-arid land regions (e.g., over Central Australia and the Sahel in Fig. 2). The adjustment in surface albedo has been further analyzed (not shown) by separating the contribution from the change in incoming SW radiation and the change in reflected SW radiation at the surface, under clear-sky and all-sky conditions. It is found that the incoming flux depends, as expected, on the cloud cover (i.e., with an increase in incoming solar radiation at the surface when the cloud cover decreases, and vice versa), while the reflected flux (which decreases over continental regions in the Northern Hemisphere, the Sahel and central Australia) is the same under clear- and all-sky conditions. This potentially suggests a link between direct or indirect CO_2-induced changes in vegetation, in turn impacting the surface reflectance (Denman et al. 2007).

The multi-model mean and inter-model spread resulting from land surface warming ($\Delta T_{s,F_p} + \Delta T_{s,0}$) is the smallest in Figs. 5c, 6b and 7b.

3.4 Summary

Considering adjustments to CO_2 does not alter climate sensitivity estimates, but does affect the quantification of feedbacks. Indeed, the multi-model mean cloud feedback is reduced by about 33 %. However, it does not affect the spread of feedbacks. Cloud feedbacks remain the main contribution to the spread of climate sensitivity, especially the tropical cloud feedbacks. To a lesser extent, the tropical WV+LR feedback also contributes to the spread of climate sensitivity estimates. The tropical cloud and WV+LR feedbacks are analyzed further in the next section. Finally, our results point to a substantial role of the residual term in the calculation of adjustments and feedbacks for the

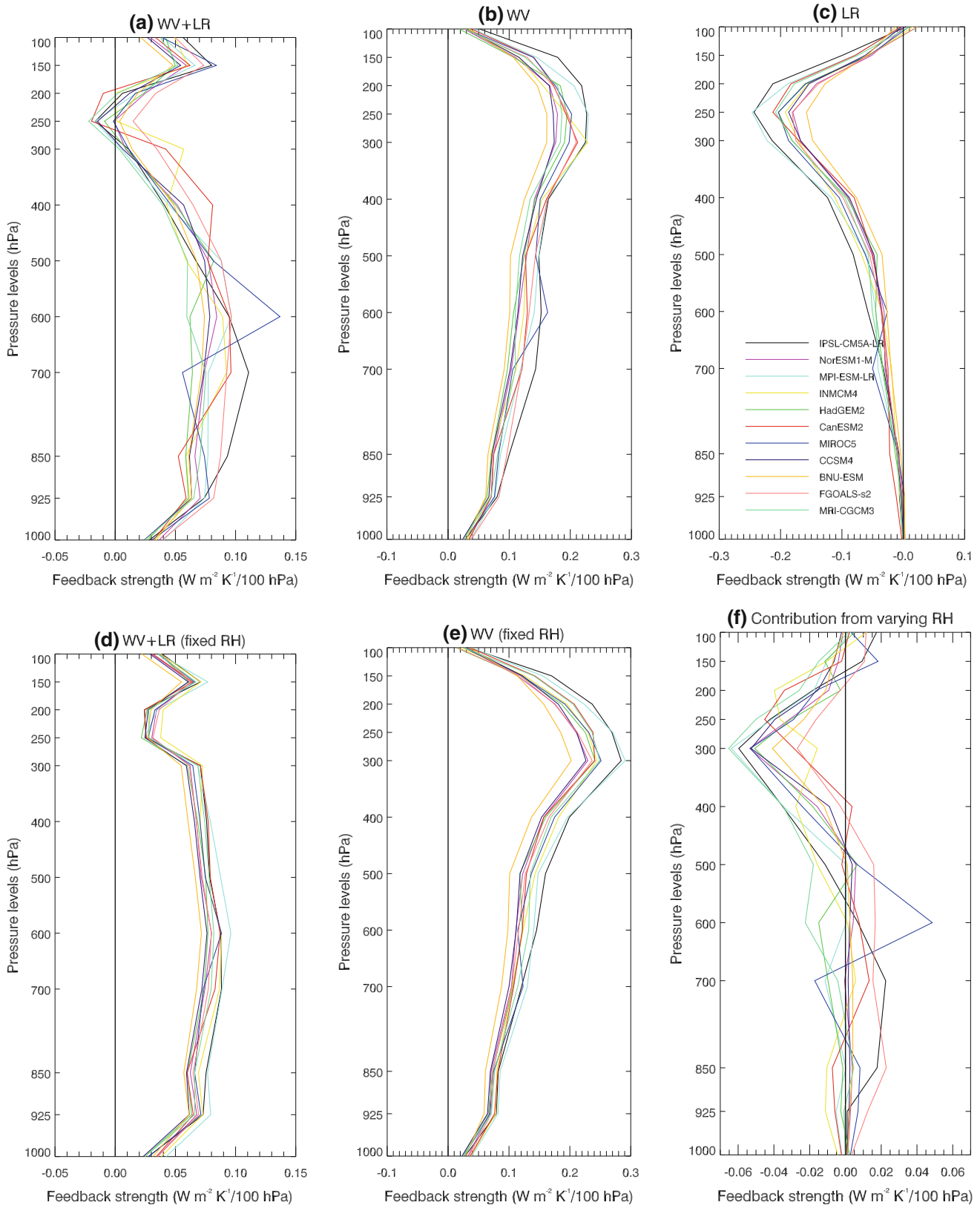

Fig. 9 Tropically-averaged, annual-mean vertical profile of the WV+LR (**a**), WV (**b**), LR (**c**), WV+LR (assuming fixed RH, **d**), WV (assuming fixed RH, **e**) feedbacks and the contribution of the WV feedback arising from changes in RH (**f**)

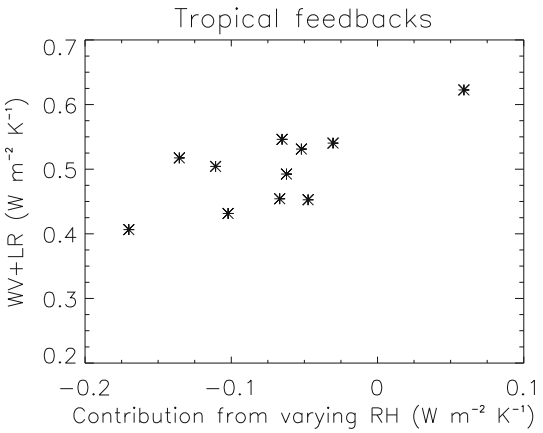

Fig. 10 Vertically-integrated, tropically-averaged, annual mean WV+LR feedback for the 11 models plotted as a function of the vertically-integrated, tropically-averaged, annual mean contribution of RH changes to the WV feedback

interpretation of inter-model spread in climate sensitivity estimates, and caution against the use of methods that include the residual term into one of the linear components (e.g., the cloud feedback of Soden and Held 2006).

4 Analysis of the spread of climate feedbacks in the tropics

4.1 The combined water vapor + lapse rate feedbacks

In this section we analyze the role of relative humidity (RH) changes to understand the amplitude and the spread of the tropically-averaged WV+LR feedback seen in Figs. 5 and 6. This is done by following the method proposed by Soden et al. (2008), whereby the water vapor feedback is recomputed by multiplying the water vapor

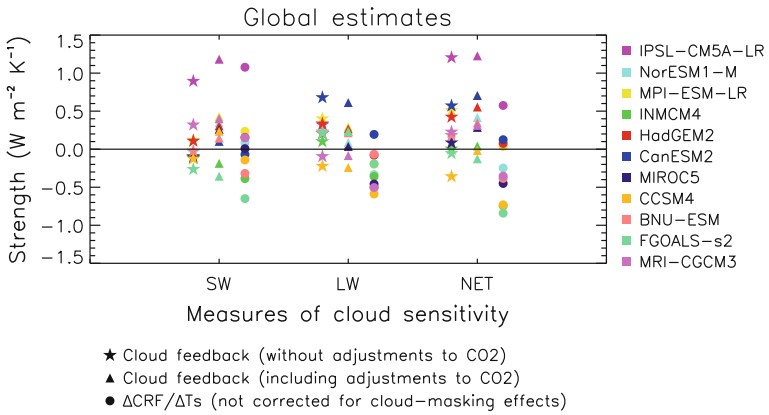

Fig. 11 Global and annual mean of three cloud sensitivity measures for the SW, LW and NET components computed for the set of models considered: the cloud feedback computed, using the NCAR model's radiative kernels, by considering the adjustments to CO_2 as part of the forcing rather than the feedbacks (*stars*), the cloud feedbacks that include the adjustments to CO_2 (*triangles*), and the changes in CRE, normalized by ΔT_s, that include the adjustments to CO_2 and that are not corrected for cloud-masking effects (*circles*)

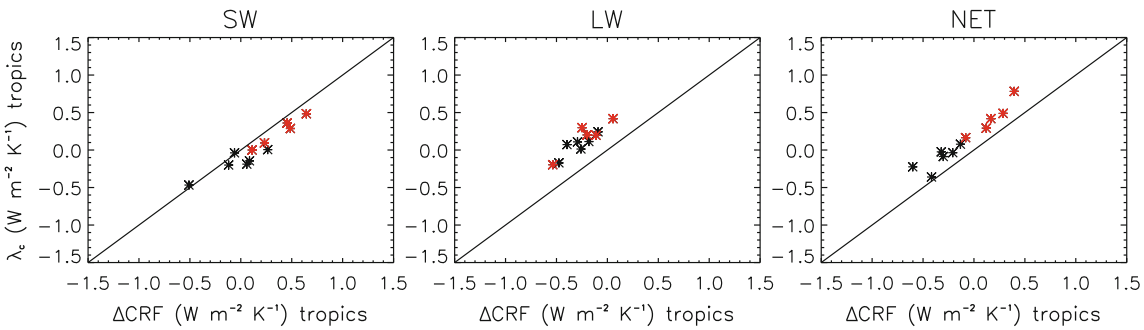

Fig. 12 Tropically-averaged cloud feedback parameter (estimated using the NCAR kernels) plotted as a function of the change in cloud radiative effect (i.e., including cloud adjustments, and without correction of the cloud-masking effect) normalized by the global mean surface temperature change over the tropics. Models that predicts a greater tropically-averaged NET cloud sensitivity (i.e., cloud feedback or change in CRE) than the tropically-averaged multi-model mean NET cloud sensitivity are shown in *red* (5 models), and those predicting a lower cloud sensitivity than the multi-model mean are in *black* (6 models)

kernel with the simulated change in atmospheric temperature and assuming no change in simulated RH (see Eqs. 20 and 21 of Soden et al. (2008) for more details). Hereafter, we refer to this feedback as the fixed-RH WV feedback (see also Held and Shell 2012 for an alternative feedback decomposition using relative humidity).

Figure 9 shows the tropically-averaged, annual-mean vertical profiles of the WV+LR (a), WV (b) and LR (c) feedbacks, as well as the fixed-RH WV+LR (d) and WV (e) feedbacks, and the contribution of RH changes to the WV feedback (computed as the differences: $\lambda_{wv}-$ fixed-RH λ_{wv}; this quantity is referred hereafter to as $\tilde{\lambda}_{wv}$, and is shown in f). As already reported in Soden and Held (2006) and Soden et al. (2008), the strength of the WV feedback is weaker by about 5 % than that computed under the assumption of fixed-RH (difference between the two vertically-integrated global-mean, annual-mean feedbacks–not shown). This difference arises primarily from the upper troposphere (above 400 hPa–compare Fig. 9b, e), and is consistent with a reduction in upper-tropospheric relative humidity in all models (as seen in Fig. 9f by negative values of $\tilde{\lambda}_{wv}$). This feature is robust over the set of models considered in this study. The spread of the WV+LR feedback computed with the assumption of fixed-RH is considerably reduced throughout the troposphere (Fig. 9d), which confirms that the spread in WV+LR is mainly controlled by departures from constant relative humidity as simulated by climate models, and that changes in relative humidity alter the radiative coupling between the water vapor and lapse rate feedback (Bony et al. 2006). Indeed, the spread of the WV+LR feedback closely follows that of $\tilde{\lambda}_{wv}$ (compare Fig. 9a, f): models with high WV+LR feedback have large increase in RH (and vice versa). This appears also when we consider the WV+LR feedback plotted as a function $\tilde{\lambda}_{wv}$ over the tropics (Fig. 10): the spread in WV+LR feedback in this region can be explained by different changes in RH simulated by the models. Note however that no clear relation arises in the mid-latitudes, and no change in RH over the poles occur (not shown). The spread of the WV+LR feedback in the mid-latitudes and the poles can however be explained by inter-model differences in LR feedbacks (not shown).

Water vapor in the upper troposphere is recognized as playing a key role in the water vapor feedback (Held and Soden 2000). The present results show however that the upper-tropospheric WV and LR feedbacks largely offset each other, with even a tendency for a greater contribution from the lapse rate resulting in a negative WV+LR feedback between 300 and 200 hPa (Fig. 9a). Below 300 hPa, however, the contribution from the positive WV feedback increases up to a maximum near 700 hPa. These results therefore suggest that the positive WV+LR feedback arises mostly from the mid-troposphere between 500 and 900 hPa.

4.2 Cloud feedbacks

About 70 % of the inter-model spread in climate sensitivity estimates arises from differing cloud feedbacks (Sect. 3) Although many areas contribute to these differences, the tropics play a prominent role in the spread of global cloud feedbacks (Fig. 7a). In this section, we analyze further the origin of this spread.

Historically, two main approaches have been used commonly to analyze the response of clouds to climate change: the diagnostic of cloud feedbacks through Partial Radiative Perturbation (PRP; Wetherald and Manabe 1988) or kernel approaches (Soden and Held 2006), and the change in CRE at the top of the atmosphere (ΔCRE) between control and perturbed climate states (Cess et al. 1990), which constitutes a much simpler diagnostic. It is recognized that owing to cloud-masking effects, the sign of ΔCRE can differ from that of the cloud feedback (a negative ΔCRE being generally associated with a neutral or weakly positive cloud feedback) and that both measures differ by an offset of about 0.3 W m^{-2} K^{-1}. (Soden and Held 2006; Soden et al. 2004).

Besides cloud-masking effects, how do cloud adjustments to CO_2 alter the relationship between ΔCRE and cloud feedbacks? Fig. 11 shows that excluding cloud adjustments from the definition of cloud feedbacks also affects the magnitude of cloud feedback estimates (compare the star and triangle symbols in Fig. 11). The multi-model mean cloud feedback is about 33 % weaker when the cloud adjustments are considered as part of forcing rather than of feedbacks. In addition, cloud feedbacks remain strongly correlated with the basic ΔCRE (i.e. the ΔCRE not corrected for cloud-masking effects and adjustments to CO_2), both at the global scale (Fig. 11) and at the tropical scale (Fig. 12). Any of these diagnostics may thus be considered for analyzing the spread of cloud feedbacks amongst models.

In the tropics, all but two models predict a positive or neutral cloud feedback (Fig. 12). To understand why some models have a larger cloud feedback than others, we use the methodology proposed by Bony et al. (2004) whereby the cloud feedback (or CRE sensitivity to surface temperature change, $\frac{\Delta CRE}{Ts}$) is composited into different dynamical regimes defined from the large-scale mid-tropospheric (500 hPa) vertical velocity (ω). By using this variable as a proxy of the large-scale tropical circulation, we discretize the tropical geographical pattern into regions of subsidence and ascendance for positive and negative values of ω, respectively.

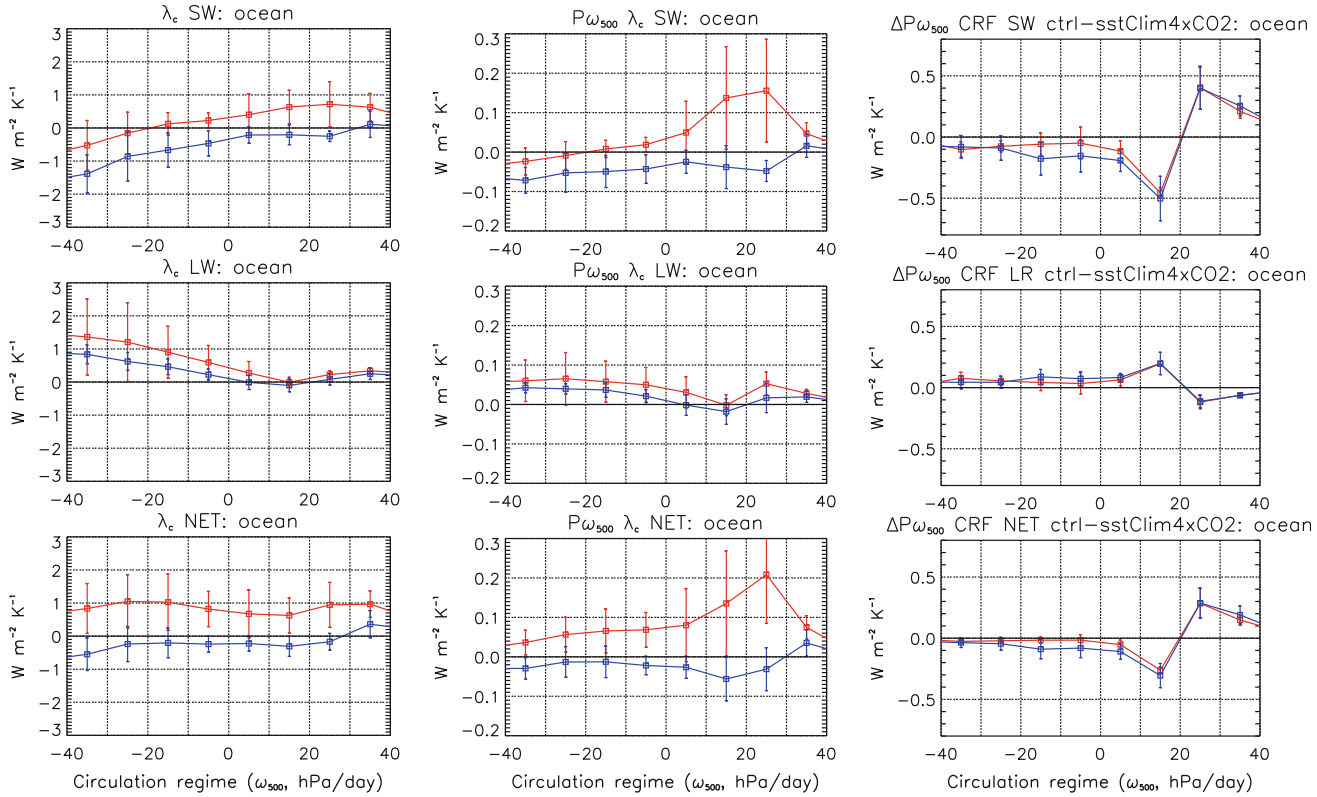

Fig. 13 SW (*top*), LW (*middle*) and NET (*bottom*) cloud feedback ($\Delta\bar{C}$) composited in each dynamical regime (*left*), the contribution from the thermodynamic component ($P_\omega \Delta C_\omega$, *middle*) and from the dynamic component ($C_\omega \Delta P_\omega$, right). Results are presented for two groups of models: models that predicts a greater tropically-averaged NET cloud feedback than the tropically-averaged multi-model mean NET cloud feedback (in *red*, 5 models), and those with a lower cloud sensitivity than the multi-model mean (in *blue*, 6 models). *Vertical bars* show the inter-model standard deviation in each group. Cloud feedbacks are estimated using the NCAR model's radiative kernels

Using this method, the tropically-averaged CRE ($\bar{C}$, in W m^{-2} K^{-1}) can be expressed as:

$$\bar{C} = \sum_{\omega} P_\omega C_\omega, \tag{30}$$

where P_ω is the probability of occurrence of regime ω and C_ω is the CRE sensitivity in the regime ω.

Now, following Eq. 30, the cloud feedback or CRE sensitivity ($\Delta\bar{C}$) is written as:

$$\Delta\bar{C} = \sum_{\omega} C_\omega \Delta P_\omega + \sum_{\omega} P_\omega \Delta C_\omega + \sum_{\omega} \Delta C_\omega \Delta P_\omega, \tag{31}$$

where ΔC_ω and ΔP_ω are the changes in C_ω and P_ω, respectively.

The first two terms of Eq. 31 quantify CRE changes that arise from large-scale circulation changes (referred to as the dynamical component), and changes in cloud-radiative properties which are not primarily related to dynamical changes (referred to as the thermodynamical component), respectively. The third term, which arises from the co-variation of dynamical and thermodynamical components, is much weaker than the two other terms. For this reason, the following analysis will be focusing on the dynamical and thermodynamical components. As done by Bony and Dufresne (2005), we group the 11 models into two categories (5 high-sensitivity models and 6 low-sensitivity models) according to their tropically-averaged NET cloud feedbacks or $\Delta CRE/\Delta T_s$ (high-sensitivity models are in red in Fig. 12). Then, the multi-model mean and inter-model spread of the dynamical and thermodynamical components of the tropical cloud feedback or $\Delta CRE/\Delta T_s$ are computed for each group. The results being very similar for both measures, and when considering land+ocean regions or ocean regions only, hereafter we present only the results for the cloud feedback over tropical oceans.

Inter-model differences in tropical NET cloud feedbacks primarily arise from the SW component. Figure 13 shows that it is the SW thermodynamical component of the feedback which best discriminates the two groups of models. All dynamical regimes, from deep convective to subsidence regimes, contribute to these differences. However, the regimes of weak subsidence and of moderate large-scale rising motion (from −10 to +30 hPa/day) have a predominant role in the spread, both because these regimes are associated with a larger contrast between the two groups of models, and mainly because of the large

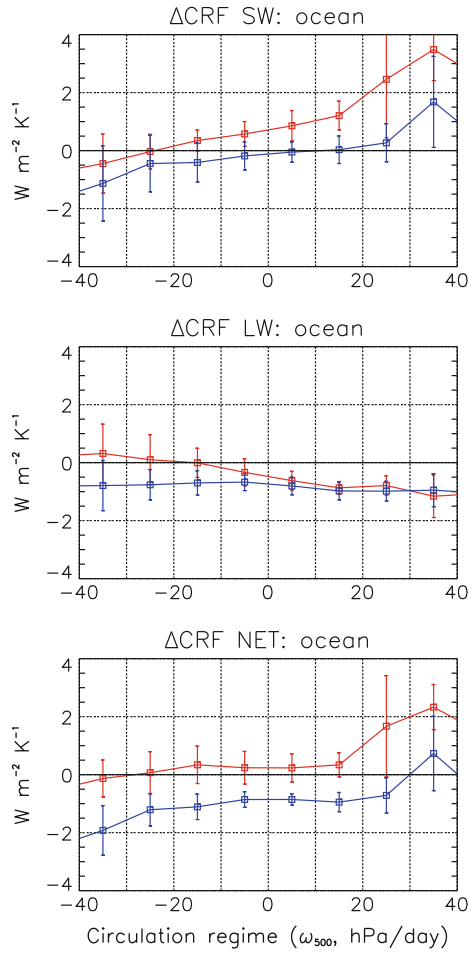

Fig. 14 Same as the left panel of Fig. 13, but for the change in CRE, normalized by the mean surface temperature change in the regime ω. The models that predict a greater change in the tropically-averaged NET CRE than its multi-model mean are in red (i.e., multi-model mean for this group), and models that predict a lower change are in blue

statistical weight of these regimes in the tropics (PDF of ω_{500}): small thermodynamic changes in these regimes have large effects on the cloud sensitivity (Fig. 13 middle panels).

To facilitate the comparison between these results and those associated with CMIP3 models, we also compute the change in CRE predicted by the two groups of models, normalized by the surface temperature change predicted within each dynamical regime as done by Bony and Dufresne (2005) (Fig. 14). As in climate change the tropical SST does not warm uniformly, the sensitivity of the SW CRE to local rather than global surface temperature changes is slightly enhanced (reduced) in subsidence (convective) regimes. The comparison of Figs. 13 and 14 also shows the offset of the LW component, and then of the NET ΔCRE, when cloud-masking effects are not accounted for. Differences in the SW component between the low and high sensitivity groups of models remain roughly similar, however, although more pronounced in regimes of subsidence.

Compared to CMIP3, the spread of tropical cloud feedbacks among CMIP5 models thus arises from a larger range of dynamical regimes, ranging from weak large-scale rising motions to subsidence regimes. Given the predominance of shallow cumulus and stratocumulus clouds in these regimes, it is likely that the responses of boundary-layer processes and shallow convection to climate change, and of the different clouds associated with them, constitute a critical component of the climate sensitivity uncertainty. Although local feedback processes might explain part of inter-model differences (Zhang and co authors 2012), the possibility that inter-model differences in cloud-radiative responses in these regimes be driven by remote responses of deep convection can not be ruled out and will have to be investigated.

5 Conclusion

In this paper, we propose an alternative approach to diagnose the radiative forcing, fast adjustments, feedbacks and the climate sensitivity in CMIP5 climate models. We use the NCAR model's radiative kernels (Shell et al. 2008) to analyze the different feedbacks and adjustments, by considering tropospheric adjustments to CO_2 and land surface warming as part of forcings rather than feedbacks. The amplitude and inter-model spread of climate sensitivity is quantified, and decomposed into different contributions related to individual adjustments and feedbacks, and into regional contributions. We show that in climate model simulations with large forcing (e.g., $4 \times CO_2$), limitations in the kernel approximation for the calculation of adjustments and feedbacks play a non-negligible role for the interpretation of inter-model spread in climate sensitivity estimates (also consistent with Jonko et al. 2012's findings). In particular, the results indicate that errors associated with the kernel method pertain mainly to the cloud component and lead to an underestimation of the multi-model mean and inter-model spread cloud-induced temperature change. We therefore caution against the use of methods in which nonlinearities are assumed minor and included into one of the linear components (e.g., the cloud feedback of Soden and Held 2006).

Taking into account the tropospheric adjustments to CO_2 does not affect the estimate of climate sensitivities. For a doubling of CO_2 concentration, the equilibrium global-mean temperature change estimates range from 1.9 to 4.4°. This range is similar to that of CMIP3 (Randall et al. 2007) and to that diagnosed by Andrews et al. (2012) for CMIP5 models using a different methodology. On the other hand, considering tropospheric adjustments to CO_2

does alter the quantification of feedbacks. The total feedback parameter is increased by 11 % compared to the previous methodology in which the adjustments to CO_2 were included in the feedbacks rather than in the forcing. The cloud feedback is the most affected, with a reduction of 33 % relative to the previous method's estimates, while the non-cloud adjustments (associated with temperature, water vapor and albedo) seem to be better understood as responses to land surface warming. The effect of cloud adjustments on feedbacks is qualitatively consistent but quantitatively weaker than found by Andrews and Forster (2008) using a different methodology to diagnose feedbacks. Moreover, and unlike Andrews and Forster (2008), the consideration of the adjustments to CO_2 does not reduce the inter-model spread of feedbacks amongst CMIP5 models. Cloud feedbacks remain the main contributors to the spread of climate sensitivity, especially tropical cloud feedbacks. The tropical combined water vapor + lapse rate feedback also contributes substantially to the spread of climate sensitivity, although to a lesser extent, mainly because of the well-known cross-model compensation between the water vapor and lapse rate feedbacks.

Further analysis of the tropical combined water vapor + lapse rate feedback shows that changes in relative humidity, as simulated by climate models, affect the radiative coupling between the water vapor and lapse rate feedback. The spread of the tropical combined water vapor + lapse rate feedback is almost entirely due to different simulated changes in relative humidity throughout the troposphere. Like in CMIP3, the spread of tropical cloud feedbacks primarily arises from differing changes in the shortwave cloud-radiative properties in regions of shallow convection (where shallow cumulus and stratocumulus clouds prevail), which in turn result from changes in the thermodynamic structure of the tropical atmosphere. Interpreting this spread in terms of local and remote physical processes and using observations to assess the relative reliability of the different model responses clearly remains a scientific challenge for the years to come. However, the wealth of CMIP5 experiments and output now available constitutes a wonderful opportunity to make progress on that matter.

Acknowledgments The research leading to these results has received funding from the European Union, Seventh Framework Programme (FP7/2007–2013) under Grant agreement no 244067 for the EUCLIPSE project, and under GA 226520 for the COMBINE project. The work was also partially funded by the ANR ClimaConf project. We acknowledge the World Climate Research Programme's Working Group on Coupled Modelling, which is responsible for CMIP, and we thank the climate modeling groups (listed in Table 1 of this paper) for producing and making available their model output. For CMIP the U.S. Department of Energy's Program for Climate Model Diagnosis and Intercomparison provides coordinating support and led development of software infrastructure in partnership with the Global Organization for Earth System Science Portals. The authors would like to acknowledge Karen Shell and Brian Soden for making the NCAR and GFDL models' radiative kernels freely available online at http://people.oregonstate.edu/~shellk/kernel.html. Finally, we thank Christelle Castet for her participation to this study, and we acknowledge the anonymous reviewers for their helpful comments and suggestions.

References

Andrews T, Forster P (2008) CO2 forcing induces semi-direct effects with consequences for climate feedback interpretations. Geophys Res Lett 35:L04,802

Andrews T, Gregory J, Webb M, Taylor K (2012) Forcing, feedbacks and climate sensitivity in CMIP5 coupled atmosphere-ocean climate models. Geophys Res Lett 39(9):L09,712

Arrhenius S (1896) On the influence of carbonic acid in the air upon the temperature of the ground. Lond Edinb Dublin Philos Mag J Sci 41(251):237–276

Block K, Mauritsen T (2013) Forcing and feedback in the MPI-ESM-LR coupled model under abruptly quadrupled CO2. J Adv Model Earth Syst (submitted)

Boer G, Yu B (2003) Climate sensitivity and climate state. Clim Dyn 21(2):167–176

Bony S, Dufresne J (2005) Marine boundary layer clouds at the heart of tropical cloud feedback uncertainties in climate models. Geophys Res Lett 23:L20,806

Bony S, Dufresne JL, Treut HL, Morcrette JJ, Senior C (2004) On dynamic and thermodynamic components of cloud changes. Clim Dyn 22:71–86

Bony S, Colman R, Kattsov V, Allan R, Bretherton C, Dufresne J, Hall A, Hallegatte S, Holland M, Ingram W, et al (2006) How well do we understand and evaluate climate change feedback processes? J Clim 19(15):3445–3482

Bony S, Stevens B, Held I, Mitchell J, Dufresne JL, Emanuel K, Friedlingstein P, Griffies S, Senior C (2013a) Carbon dioxide and climate: perspectives on a scientific assessment. In: Hurrel J, Asran G (eds) Climate science for serving society: research, modelling and prediction priorities. Springer, Monograph

Bony S, Bellon G, Klocke D, Sherwood S, Fermepin S, Denvil S (2013b) Robust direct effect of carbon dioxide on tropical circulation and regional precipitation. Nat Geosci (in press)

Cess R, Potter G, Blanchet J, Boer G, Del Genio A, Deque M, Dymnikov V, Galin V, Gates W, Ghan S, et al (1990) Intercomparison and interpretation of climate feedback processes in 19 atmospheric general circulation models. J Geophys Res 95(16):601,216

Charney JG, et al (1979) Carbon dioxide and climate: a scientific assessment : report of an ad hoc study group on carbon dioxide and climate, woods hole, Massachusetts, July 23–27, 1979 to the climate research board, assembly of mathematical and physical sciences, National Research Council. National Academy of Sciences: available from Climate Research Board, http://books.google.com/books?id=cj0rAAAAYAAJ

Colman R, McAvaney B (2011) On tropospheric adjustment to forcing and climate feedbacks. Clim Dyn 36(9):1649–1658

Denman K, Brasseur G, Chidthaisong A, Ciais P, Cox P, Dickinson R, Hauglustaine D, Heinze C, Holland E, Jacob D, et al (2007) Couplings between changes in the climate system and biogeochemistry. Climate change 2007: the physical science basis contribution of working group I to the fourth assessment report of the intergovernmental panel on climate change [Solomon S, D Qin, M Manning, Z Chen, M Marquis, KB Averyt, MTignor and HL Miller (eds)]

Dufresne JL, Bony S (2008) An assessment of the primary sources of spread of global warming estimates from coupled atmosphere-ocean models. J Clim 21:5135–5144

Forster P, Ramaswamy V, Artaxo P, Berntsen T, Betts R, Fahey D, Haywood J, Lean J, Lowe D, Myhre G, et al (2007) Changes in atmospheric constituents and in radiative forcing. Climate change 2007: the physical science basis contribution of working group I to the fourth assessment report of the intergovernmental panel on climate change [Solomon, S, D Qin, M Manning, Z Chen, M Marquis, KB Averyt, MTignor and HL Miller (eds)]

Gregory J, Webb M (2008) Tropospheric adjustment induces a cloud component in CO2 forcing. J Clim 21:58–71

Gregory JM, Ingram WJ, Palmer MA, Jones GS, Thorpe PASRB, Lowe JA, Johns TC, Williams KD (2004) A new method for diagnosing radiative forcing and climate sensitivity. Geophys Res Lett 31:L03,205

Hansen J, Sato M, Ruedy R, Nazarenko L, Lacis A, Schmidt G, Russell G, Aleinov I, Bauer M, Bauer S, et al (2005) Efficacy of climate forcings. J Geophys Res 110(D18):D18,104

Held I, Soden B (2000) Water vapor feedback and global warming 1. Annu Rev Energy Environ 25(1):441–475

Held IM, Shell KM (2012) Using relative humidity as a state variable in climate feedback analysis. J Clim 25(8):2578–2582

Jonko A, Shell K, Sanderson B, Danabasoglu G (2012) Climate feedbacks in CCSM3 under changing CO2 forcing. Part I: adapting the linear radiative kernel technique to feedback calculations for a broad range of forcings. J Clim 25(15): 5260–5272

Knutti R, Hegerl G (2008) The equilibrium sensitivity of the earth's temperature to radiation changes. Nat Geosci 1(11):735–743

Mauritsen T, Graversen RG, Klocke D, Langen PL, Bjorn S, Tomassini L (2013) Climate feedback efficiency and synergy. Clim Dyn (submitted)

Randall D, Wood R, Bony S, Colman R, Fichefet T, Fyfe J, Kattsov V, Pitman A, Shukla J, Srinivasan J, et al (2007) Climate models and their evaluation. Clim Change 323

Shell KM, Kiehl JT, Shields CA (2008) Using the radiative kernel technique to calculate climate feedbacks in NCAR's community atmospheric model. J Clim 21:2269–2282

Soden B, Held I (2006) An assessment of climate feedbacks in coupled ocean-atmosphere models. J Clim 19(14):3354–3360

Soden B, Held I, Colman R, Shell K, Kiehl J, Shields C (2008) Quantifying climate feedbacks using radiative kernels. J Clim 21(14):3504–3520

Soden BJ, Broccoli AJ, Hemler RS (2004) On the use of cloud forcing to estimate cloud feedback. J Clim 19:3661–3665

Taylor KE, Stouffer RJ, Meehl GA (2012) An overview of CMIP5 and the experiment design. Bull Am Meteorol Soc 93(4): 485–498. doi:10.1175/BAMS-D-11-00094.1

Webb M, Senior C, Sexton D, Ingram W, Williams K, Ringer M, McAvaney B, Colman R, Soden B, Gudgel R, et al (2006) On the contribution of local feedback mechanisms to the range of climate sensitivity in two GCM ensembles. Clim Dyn 27(1): 17–38

Wetherald RT, Manabe S (1988) Cloud feedback processes in a general circulation model. J Atmos Sci 45:1397–1415

Zhang M, et al. (2012) CGILS: first results from an international project to understand the physical mechanisms of low cloud feedbacks in general circulation models. Bull Am Meteorol Soc (submitted)